Simulation–Based Optimal Design of Induction Machine Drives

By

Maryam Salimi

A thesis submitted to the Faculty of Graduate Studies of
The University of Manitoba
in partial fulfillment of the requirements for the degree of

Master of Science

Department of Electrical and Computer Engineering
University of Manitoba
Winnipeg, Manitoba

Abstract

An electric motor drive is a power-electronic based system that is used to precisely control the position, speed or torque developed by motor. With the growing complexity of drive systems and the expansion of the use of fast acting power-electronic controllers, computer simulation models are used instead of an explicit mathematical description of a complex system.

The aim of this research is to study the use of the simulation based design method for advanced motor drives. The major problem for simulation of a drive system performance is the presence of both fast and slow dynamics in its response that result in relatively long time simulations with a small time step. Moreover, the simulation-based optimal design has a repetitive nature. Therefore, the simulation-based optimal design of a drive system is massively time consuming and require extensive computing resources. In this research reduced intensity computer models are used to overcome this problem.

Acknowledgments

First and foremost I would like to offer my sincerest gratitude to my advisor, Professor Shaahin Filizadeh, for his supervision, advice and encouragement during all stage of my Master's program. Not just as an advisor, Dr. Filizadeh and his wife, dear Leila, are our best friends who taught me enthusiastically how to overcome the difficulties of immigration and also how to make my decision for the most dramatic happening of my life, my marriage.

I would like to acknowledge the financial support from Manitoba Hydro and MITACS Internship Program. I also wish to thank the staffs of Manitoba HVDC Research Centre who were my kind colleagues during last year. Especially I would like to appreciate Dr. Rohitha Jayasinghe and Dr. Dharshana Muthumuni who were my supervisors and shared generously their experience and made a pleasant work place for me.

I do not know how to put my appreciation feeling into words for my parents, who tolerate my absence and support me lovingly to make me able to pursue my goals and have a better life.

Finally, I would like to express my thankfulness for my dear Ehsan, who was my best friend during the first year of my studies and is my beloved husband now. I want to thank him for his emotional support, responsibility, sense of humor and his presence that has made my life incredibly happy.

To

My beloved parents

and

My dear Ehsan

Contents

List of Tables

List of Figures

Chapter 1

Introduction

Electric motors are workhorses of the modern society. They are used in a wide spectrum of power levels ranging from fraction of a watt to several mega-watts. Electric motors are found in a wide variety of forms, e.g. ac or dc, single-phase or three-phase, etc. Conventional dc motors are highly efficient and their characteristics make them suitable for use over a wide range of operating conditions. They dominated motion control applications for a long time due to their appealing controllability features. However, dc motors use commutator and brushes, which are exposed to wear and tear and require maintenance [1]. Thanks to modern power electronics and control technology, ac motor drives have improved significantly. Use of power electronic devices along with sophisticated control circuitry has led to the development of advanced methods for high-precision torque and speed control of ac machines in high-power applications. The induction motors are the most commonly used ac motor in industrial applications because of their simplicity, rugged construction, high efficiency and high overload capacity. Furthermore operating without commutator and brushes results in relatively low

maintenance costs; they can also work in explosive environments since no spark is produced during their operation [2],[3].

At sufficiently high power levels, electric motor drives will become major loads for a utility grid and their operation will have significant impacts on the network. Moreover, use of power electronic converters for their operation often causes harmonic and power quality issues that need to be taken into consideration both during their design and operation [4]. Therefore study of the control design methodologies and improvement of the adverse impacts of electric motors on the network is inevitable.

The scope of this thesis is first to study power electronic based induction motor drives that are based on the dynamic model of the machine. This research aims to develop computer simulation platforms and methods for optimal design of advanced electric motor drive systems. Optimal design will be done with a view to enhance the dynamic performance of the drive system during load changes and also to minimize the adverse impacts of the steady state operation of drive on its feeding power system to lower power quality consequences. To lessen the computational intensity of drive simulation, low-intensity average-value and mathematical models will be explored and their use in the simulation-based optimal design of motor drive systems will be demonstrated.

1.1 Motivation and Background

1.1.1 Power electronics based induction machine drives

The utility power supply has constant frequency quantities. Since the speed of ac machines is proportional to the frequency of input quantities, they operate with a fixed speed when supplied directly from the mains. Therefore, introduction of variable speed drives increases the automation and productivity and efficiency of ac machines. A modern electric motor drive is a complex power-electronic system that is used to interface an electric motor with the utility grid to adjust the input parameters of the motor, e.g. terminal voltage, frequency or current. By properly adjusting the terminal parameters of the motor, a drive system enables the motor to match the requirements of the load precisely. Motor drives come in a variety of forms and have varying levels of complexity depending on their applications. There are numerous control strategies that have been formulated for various motor drives. They are developed depending on the motor's performance and the viability and cost of its real implementation [5].

In general, the control methodologies applied for induction machine drives can be categorized into steady state and dynamics-based on the underlying model of the machine. In the former, the control methodology for the drive system is drawn from the steady state operation of the machine. Voltage-frequency (V/f) is the simplest control methodology that acts by imposing a constant relation between the voltage and frequency. Although this drive performs satisfactorily in steady state, the transient performance cannot be predicted or controlled precisely. In practice, for low performance

applications, open loop voltage/frequency control strategies are employed. In the latter category of motor drives, a mathematical model of the machine that is valid in both transient and steady state is used to develop control strategies for the drive. Even though these control strategies require massive computations due to the complexity of the algorithm, the resulting drives offer superior performance and are suited for high-precision applications [6], [7].

Considering dynamics-based induction machine drives, the field oriented control (FOC) (also known as the vector control) and the direct torque control (DTC) are used as high-performance motion control drives. The concepts of both FOC and DTC have introduced a new possibility to have ac drives of similar flexibility to dc drives because of the independent control of the flux and torque and consequently in their dynamic performance. In other words, these control strategies allow the torque and flux to be decoupled and controlled independently. In dc machines this decoupling is obtained in an electromagnetic way by orienting the current with respect to the stator flux using a commutator. However, in ac machines under FOC or DTC regimes, such decoupling is obtained by implementing mathematical transformations, without using a commutator [5]-[9].

1.1.2 Simulation-Based Optimal Design

When designing a control system to drive an induction machine, a major issue is the selection the values of the system parameters (control system parameters, size of the system elements, etc) in order to optimize the system performance according to the machine application. Moreover, due to the nonlinear switching structure of the power

electronic devices in drive system and complicated nature of the control scheme, selection of the optimal parameter for the drive system is a time consuming and difficult process. Although by trial and error methods through several simulations and using engineering judgement, one can acquire the system parameters that result in stable and satisfactory performance of the system, obtaining the optimal results that fulfil the desired objectives by this method requires extra design cost and length [10], [11].

One of the methods that can reduce the number of required simulation runs with minimum human interaction is to employ the technique of optimization enabled electromagnetic transient simulation. In this method, a nonlinear optimization algorithm is used to carry out a sequence of runs on an electromagnetic transient simulator. During every simulation run, the performance of the system is evaluated by scrutinizing the simulation results; to measure how closely the design objectives are satisfied an objective function is evaluated. Objective functions are typically designed so that a smaller value of the objective functions indicates that the simulation results are closer to the desired values [10]- [15].

However, for such nonlinear and complex systems as ac motor drives, developing an explicit objective function in terms of the system parameters is complicated and nearly impossible. Therefore in simulation based optimization methods, instead of expressing an analytical form for objective function, the objective function is evaluated based on the simulation results achieved for each set of parameter values. The simulation based optimal design method is schematically shown in Figure 1-1 [10]- [12].

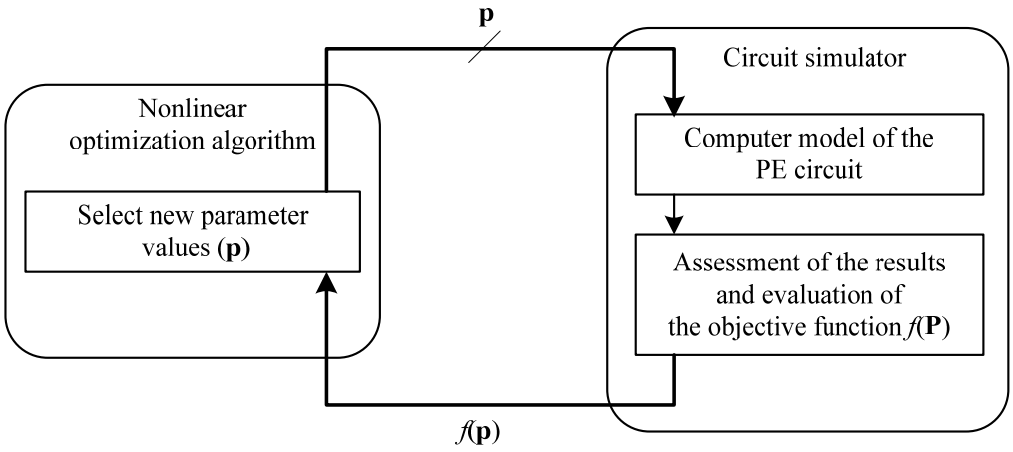

Figure 1-1 Simulation-based optimal design

The benefits of the simulation-based design procedure include design automation, shorter design cycles, uncompromised design, and optimal performance [13]-[15]. This procedure has already been successfully applied to the design of highly complex power systems [16].

1.2 Problem Definition and Research Objectives

Modeling and simulation of power and power electronic-based systems are essential steps in design and validation of such systems and applications. Although an acceptable level of experience exists in the use of the simulation-based design method for power systems, such experience has not been developed in the design of advanced motor drive systems [16]. Nowadays there are several simulation tools that can be used for simulation of electric drive systems. The PSCAD/EMTDC is a powerful transient simulator that enables the user to model power electronic components and modules in detail. This simulator is capable of simulating system performance during the steady state and fast

transients by choosing a suitable time step. However using the detailed models usually requires an excessive amount of CPU time.

The major challenge for simulation of the transient performance of a modern drive system compared to a typical power system is that a drive system consists of both mechanical subsystems and power electronic converters. Mechanical subsystems always have large time constants due to their slow nature that leads to longer transients. On the other hand, switching devices are operating with a high switching frequency that requires a small simulation time step to achieve reasonable results. This means that the simulation must run for a relatively long time with a small time step. Moreover, the simulation-based optimal design procedure is a repetitive process involving a large number of time-consuming simulations. Therefore, it is expected that the simulation-based design of a drive system be massively time consuming and require extensive computations.

This research aims to study the use of the simulation based optimal methods for the optimal design of high performance induction motor drives. In particular, the following objectives will be pursued.

1.2.1 Adoption of the design procedure for the drive systems

As the first stage of this research, the dynamic model of induction machine along with the control methodologies for two high performance drive systems will be studied. Then the design specifications for these drive systems and methods for their translation into objective function will be considered. An integral and creative part of the design procedure using simulation experiments is to develop a suitable objective function. Development of suitable objective functions that encapsulate the design specifications is

not a trivial task and requires experience and close observation of the simulations. Preliminary designs will be done to ensure that specifications for drive systems can be adequately and accurately represented in terms of measurable objective functions.

1.2.2 Development of reduced-intensity computer models

As stated earlier, using detailed switching models in simulation of power electronic-based motor drives leads to significant increase in simulation time and intensity. The next stage of the research presented in this thesis is to develop computationally simplified models of the high frequency power electronic converters used in a drive system. To remove the fast switching events in simulation of the drive system, equivalent circuits are developed to be used instead of the power electronic switch models. Dynamic average modeling and mathematical modeling of power electronic systems, which are based on the controlled voltage and current sources, are considered as potential solutions to reduce the simulation intensity.

1.3 Thesis Organization

This thesis continues in Chapter 2 with developing a mathematical model for a three-phase induction machine that is valid in both transient and steady state operation of the motor. Chapter 3 introduces a widely used power electronic drive circuit that connects the utility power supply to the ac motor via an intermediate dc link. It follows with explanation of each power conversion stage of this drive in detail mostly regarding to inversion and its functional operation. Then in the next two following chapters (Chapter 4 and

Chapter 5) two different high performance control methodologies for driving the induction machine will be presented.

In Chapter 4, vector controlled induction motor drives are presented. In this chapter the mathematical principle of vector control methodology is first explained. Then the modeling of two prevalent types of vector control schemes, which are direct vector control and indirect vector control, is introduced. In this thesis the indirect vector control will be employed to implement the simulation based optimal design of induction motor drive using the PSCAD/EMTDC simulator.

Chapter 5 is devoted to direct torque control induction machine drives. In this chapter the principle of direct torque control along with different categories of this control scheme is studied. In this research it is intended to implement the simulation based optimal design of DTC scheme operating at constant switching frequency.

Chapter 6 provides dynamic average value modeling and mathematical modeling of the power electronic inverter as solutions to reduce computational intensity of the network and therefore the simulation time.

Chapter 7 presents the concluding remarks and contributions made in this research. Moreover, the related subjects that can extend this research are proposed in this chapter.

Chapter 2

Induction Machine Modeling

In order to develop high-performance drive systems for an induction machine, its dynamic model must be known. The dynamic model of the machine is an accurate representation of its dynamic behavior and can be used to predict it during transient and steady state operation. Such a model can be obtained by means of the two-axis theory of electrical machines [17], [18].

In this chapter the model of a three-phase induction machine is developed starting with an explanation of the principles of its operation. The voltage and torque equations in terms of machine variables will be derived. Then Park's transformation will be applied in order to eliminate the time dependency and therefore to simplify the induction machine torque and voltage expressions. Next the steady state model is obtained from the voltage equations in an arbitrary reference frame [18].

The following assumptions are made to simplify the modeling procedure:

- Iron losses are neglected: a portion of the losses in electrical machines is the losses in the iron core including hysteresis loss and eddy current loss. For

simplicity the iron used in the machine assumed to have zero hysteresis and infinite resistance; therefore the iron losses are neglected. In practice, use of high-quality magnetic materials reduces the hysteresis losses and by constructing the machine using insulated laminates, the eddy current loss is minimized.

- The permeability of the iron parts is infinite: reluctance of the iron parts in the machine is negligible compared with the reluctance of the air gap. This is due to the high permeability of the iron.
- The machine has symmetrical *P*-pole, three phase sinusoidally distributed windings.
- Slotting effects are neglected: the rotor is assumed to have a cylindrical shape although slots make it slightly different.
- The stator and the rotor windings are simplified as a single multi-turn full pitch coil situated on the two sides of the air gap.
- Flux density is radial in the air gap

2.1 Basic principles of three phase induction machine

In an induction machine a rotating magnetic field is produced when balanced three phase voltages are applied to three phase windings of the stator displaced in space by 120º electrical. This rotating magnetic field has a sinusoidally distributed intensity with a constant peak and rotates at the supply frequency. Unless the rotor rotates at the exact

angular speed as the stator's rotating field, the rotor windings will experience a varying flux linkage and thereby induced voltage. As the rotor windings are short circuited, currents will start circulating in them, producing a reaction. As known from Lenz's law, the reaction is to counter the source of the flux change. These currents will disappear if the rotor rotates in the same direction as rotating magnetic field, and with the same speed. Thus the rotor starts to rotate, in an attempt to catch up with the rotating magnetic field. If the relative speed between these two become zero then there will be no emf, and the rotor currents will be zero resulting in zero torque production. Depending on the shaft load the rotor will always settle at a speed ω_r, which is less than the supply frequency ω_e. This differential speed is called the slip speed ω_s, the relationship between ω_e and ω_s is given as follows.

$$\omega_s = \omega_e - \omega_r \tag{2.1}$$

If the machine has P poles, the mechanical speed of the shaft is ω_m and is given as follows [1].

$$\omega_r = \frac{P}{2}\omega_m \tag{2.2}$$

2.2 Voltage equations

Consider a three-phase two-pole induction machine as shown in Figure 2-1.

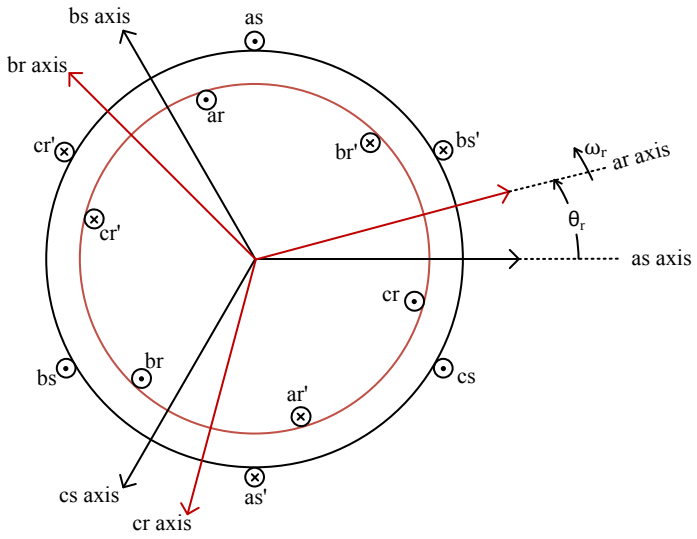

Figure 2-1 Two-pole three-phase symmetrical induction machine

The stator and rotor windings are represented using equivalent sinusoidally distributed windings, with N_s and N_r equivalent turns and resistances R_s and R_r respectively. The stator voltage equations in the stationary reference fixed to the stator frame can be expressed as follows.

$$v_{sa}(t) = R_s i_{sa}(t) + \frac{d\lambda_{sa}(t)}{dt}$$

$$v_{sb}(t) = R_s i_{sb}(t) + \frac{d\lambda_{sb}(t)}{dt} \qquad (2.3)$$

$$v_{sc}(t) = R_s i_{sc}(t) + \frac{d\lambda_{sc}(t)}{dt}$$

Similarly the rotor voltage equations in the reference frame fixed to the rotor are as follows.

$$v_{ra}(t) = R_r i_{ra}(t) + \frac{d\lambda_{ra}(t)}{dt}$$

$$v_{rb}(t) = R_r i_{rb}(t) + \frac{d\lambda_{rb}(t)}{dt} \tag{2.4}$$

$$v_{rc}(t) = R_r i_{rc}(t) + \frac{d\lambda_{rc}(t)}{dt}$$

where:

$v_{sa}, v_{sb}, v_{sc}, v_{ra}, v_{rb}, v_{rc}$ are the stator and rotor three phase voltages,

$\lambda_{sa}, \lambda_{sb}, \lambda_{sc}, \lambda_{ra}, \lambda_{rb}, \lambda_{rc}$ are the stator and rotor three phase linkage fluxes, and

$i_{sa}, i_{sb}, i_{sc}, i_{ra}, i_{rb}, i_{rc}$ are the stator and rotor three phase currents.

The instantaneous flux linkage per phase of the stator and the rotor can be expressed as shown below.

$$\begin{bmatrix} \lambda_{abcs} \\ \lambda_{abcr} \end{bmatrix} = \begin{bmatrix} L_s & L_{sr} \\ (L_{sr})^T & L_r \end{bmatrix} \cdot \begin{bmatrix} i_{abcs} \\ i_{abcr} \end{bmatrix} \tag{2.5}$$

where the winding inductances L_s, L_r and L_{sr} are as follows.

$$L_s = \begin{bmatrix} L_{ls} + L_{ms} & -\frac{1}{2}L_{ms} & -\frac{1}{2}L_{ms} \\ -\frac{1}{2}L_{ms} & L_{ls} + L_{ms} & -\frac{1}{2}L_{ms} \\ -\frac{1}{2}L_{ms} & -\frac{1}{2}L_{ms} & L_{ls} + L_{ms} \end{bmatrix} \tag{2.6}$$

$$L_r = \begin{bmatrix} L_{lr} + L_{mr} & -\frac{1}{2}L_{mr} & -\frac{1}{2}L_{mr} \\ -\frac{1}{2}L_{ms} & L_{lr} + L_{mr} & -\frac{1}{2}L_{mr} \\ -\frac{1}{2}L_{mr} & -\frac{1}{2}L_{mr} & L_{lr} + L_{mr} \end{bmatrix} \tag{2.7}$$

$$L_{sr} = L_{sr}\begin{bmatrix} \cos\theta_r & \cos(\theta_r + \frac{2\pi}{3}) & \cos(\theta_r - \frac{2\pi}{3}) \\ \cos(\theta_r - \frac{2\pi}{3}) & \cos\theta_r & \cos(\theta_r + \frac{2\pi}{3}) \\ \cos(\theta_r + \frac{2\pi}{3}) & \cos(\theta_r - \frac{2\pi}{3}) & \cos\theta_r \end{bmatrix} \tag{2.8}$$

In the above equations, L_{ls} and L_{lr} are the stator and rotor leakage inductances respectively, and L_{ms} and L_{mr} are the stator and rotor magnetizing inductances respectively.

To express the voltage equations, it is more convenient to transfer all rotor quantities to the stator winding side by a suitable turn ratio similar to what is commonly done for transformers; therefore the rotor current, voltage, and flux reflected to the stator side can be defined as follows.

$$i'_{abcr} = \frac{N_r}{N_s} \cdot i_{abcr} \tag{2.9}$$

$$v'_{abcr} = \frac{N_s}{N_r} \cdot v_{abcr} \tag{2.10}$$

$$\lambda'_{abcr} = \frac{N_s}{N_r} \cdot \lambda_{abcr} \tag{2.11}$$

Consequently the transferred magnetizing and mutual inductances of the rotor are obtained as follows.

$$L'_{sr} = \frac{N_s}{N_r} \cdot L_{sr} \tag{2.12}$$

$$L'_r = \left(\frac{N_s}{N_r} \right)^2 \cdot L_r \tag{2.13}$$

$$R'_r = \left(\frac{N_s}{N_r} \right)^2 \cdot R_r \tag{2.14}$$

Substituting the reflected quantities in (2.5) the flux linkages are stated as given below.

$$\begin{bmatrix} \lambda_{abcs} \\ \lambda'_{abcr} \end{bmatrix} = \begin{bmatrix} L_s & L'_{sr} \\ \left(L'_{sr}\right)^T & L_r \end{bmatrix} \cdot \begin{bmatrix} i_{abcs} \\ i'_{abcr} \end{bmatrix} \tag{2.15}$$

A matrix notation can be used to express the voltage equations in terms of currents and machine variables referred to the stator side in a compact format as given below.

$$\begin{bmatrix} v_{abcs} \\ v'_{abcr} \end{bmatrix} = \begin{bmatrix} R_s + pL_s & pL'_{sr} \\ p\left(L'_{sr}\right)^T & R'_r + pL'_r \end{bmatrix} \cdot \begin{bmatrix} i_{abcs} \\ i'_{abcr} \end{bmatrix} \tag{2.16}$$

where p is the derivative operator, i.e. $p = d/dt$.

2.3 Torque equations

Generally the energy stored in the coupling field of a linear electromagnetic system with K electrical inputs can be expressed as

$$W_f(i_1, i_2, ..., i_K) = \frac{1}{2} \sum_{i=1}^{K} \sum_{j=1}^{K} L_{ij} i_i i_j \tag{2.17}$$

where L_{ii} is the self inductance of winding i and L_{ij} is the mutual inductance of winding i and j. Note that the energy stored in the leakage inductances is not a part of the

energy stored in the coupling field; therefore, the energy stored in the coupling field of an induction machine can be obtained by subtracting the leakage terms as follows.

$$W_f = \frac{1}{2}(i_{abcs})^T (L_s - L_{ls}I) i_{abcs} + (i_{abcs})^T L'_{sr} i'_{abcr} + \frac{1}{2}(i'_{abcr})^T (L'_r - L'_{lr}I) i'_{abcr} \qquad (2.18)$$

With the assumption of linearity for the magnetic circuit, the field energy is equal to its co-energy W_c. Further for a *P*-pole machine, the electrical angular displacement θ_r is related to the actual mechanical displacement of the rotor as follows.

$$\theta_r = \left(\frac{P}{2}\right) \cdot \theta_{rm} \qquad (2.19)$$

where θ_{rm} is the actual displacement of the rotor in mechanical radians. The electromagnetic torque can therefore be evaluated from the following expression.

$$T_e(i_j, \theta_r) = \left(\frac{P}{2}\right) \frac{\partial W_c(i_j, \theta_r)}{\partial \theta_r} \qquad (2.20)$$

Substituting W_f from (2.18) into (2.20) the torque equation in terms of electrical quantities will be derived as follows.

$$T_e = \left(\frac{P}{2}\right) (i_{abcs})^T \frac{\partial (L'_{sr})}{\partial \theta_r} i'_{abcr} \qquad (2.21)$$

On the other hand the torque and rotor speed are the mechanical outputs of the motor and they are related by the following equation.

$$T_e = J\left(\frac{2}{P}\right)\frac{d}{dt}\omega_r + B\omega_r + T_L \qquad (2.22)$$

where J is the inertia of the rotor, T_L is the active load torque, and B is the damping ratio.

The above torque equations along with the terminal voltage equations describe the dynamic behavior of the induction machine.

2.4 Park's transformation

Since the flux equation (2.5) and accordingly the voltage and torque equations of the machine (2.16) and (2.21) contain inductance terms that are functions of time, it is desired to remove such time-dependence to make simulation and analysis easier. This is done using what is commonly referred to as reference frame transformation or Park's transformation [18], [19].

The physical implication of Park's transform is transferring three windings of an induction machine to only two fictitious windings (known as the direct (d) and quadrature (q) axes) as illustrated in Figure 2-2 (Note that since the induction machine windings are symmetrical the zero component is zero). Therefore, by applying this transformation to the induction machine voltage equations, an equivalent dq set of equations is obtained.

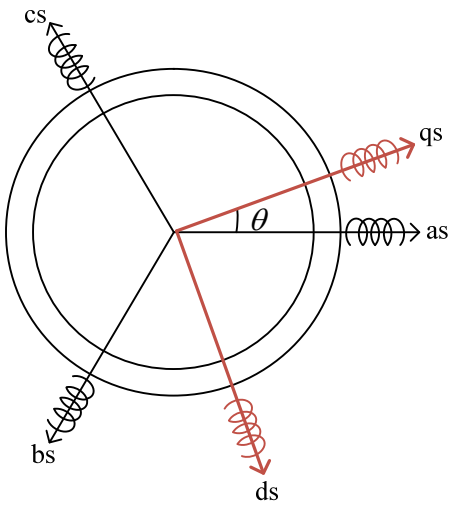

Figure 2-2 Scheme of the equivalence physic transformation

It is assumed that the position of the reference frame (relative to the axis of the quantities that are transformed) is denoted by θ as shown in Fig. 2-2 where $\omega = \frac{d\theta}{dt}$

The transformation matrix K_s for the stator quantities is presented in (2.23) and (2.24)

$$F_{qd0s} = K_s F_{abcs} \tag{2.23}$$

$$K_s = \frac{2}{3}\begin{bmatrix} \cos(\theta) & \cos(\theta - \frac{2\pi}{3}) & \cos(\theta + \frac{2\pi}{3}) \\ \sin(\theta) & \sin(\theta - \frac{2\pi}{3}) & \sin(\theta + \frac{2\pi}{3}) \\ \frac{1}{2} & \frac{1}{2} & \frac{1}{2} \end{bmatrix} \tag{2.24}$$

The Park's transformation of the three phase variables of the rotor circuits to the same reference frame is

$$F'_{qd0r} = K_r F'_{abcr} \tag{2.25}$$

$$K_r = \frac{2}{3}\begin{bmatrix} \cos(\beta) & \cos(\theta - \frac{2\pi}{3}) & \cos(\beta + \frac{2\pi}{3}) \\ \sin(\beta) & \sin(\beta - \frac{2\pi}{3}) & \sin(\beta + \frac{2\pi}{3}) \\ \frac{1}{2} & \frac{1}{2} & \frac{1}{2} \end{bmatrix} \tag{2.26}$$

where

$$\beta = \theta - \theta_r \tag{2.27}$$

is the angle between the rotor a-axis and the reference frame q-axis, and θ_r is defined by $\omega_r = \frac{d\theta_r}{dt}$.

In general, the angle θ and its time derivative are unspecified and the corresponding reference frame is called an arbitrary reference frame. Using the transformation to the arbitrary reference frame, the flux linkage equations can be expressed as follows.

$$\begin{bmatrix} \lambda_{qd0s} \\ \lambda'_{qd0r} \end{bmatrix} = \begin{bmatrix} K_s L_s (K_s)^{-1} & K_s L'_{sr} (K_r)^{-1} \\ K_r \left(L'_{sr}\right)^T (K_s)^{-1} & K_r L'_r (K_r)^{-1} \end{bmatrix} \cdot \begin{bmatrix} i_{qd0s} \\ i'_{qd0r} \end{bmatrix} \tag{2.28}$$

Simplifying this equation the linkage flux expression will be as follows.

$$\begin{bmatrix} \lambda_{qs} \\ \lambda_{ds} \\ \lambda_{0s} \\ \lambda'_{qr} \\ \lambda'_{dr} \\ \lambda'_{0r} \end{bmatrix} = \begin{bmatrix} L_{ls}+L_M & 0 & 0 & L_M & 0 & 0 \\ 0 & L_{ls}+L_M & 0 & 0 & L_M & 0 \\ 0 & 0 & L_{ls} & 0 & 0 & 0 \\ L_M & 0 & 0 & L'_{lr}+L_M & 0 & 0 \\ 0 & L_M & 0 & 0 & L'_{lr}+L_M & 0 \\ 0 & 0 & 0 & 0 & 0 & L'_{lr} \end{bmatrix} \cdot \begin{bmatrix} i_{qs} \\ i_{ds} \\ i_{0s} \\ i'_{qr} \\ i'_{dr} \\ i'_{0r} \end{bmatrix} \tag{2.29}$$

where $L_M = \frac{3}{2} L_{ms}$.

The dq0 components of the stator and rotor voltages in arbitrary reference frame are listed below.

$$v_{qs} = R_s i_{qs} + \omega \lambda_{ds} + p \lambda_{qs} \tag{2.30}$$

$$v_{ds} = R_s i_{ds} - \omega \lambda_{qs} + p \lambda_{ds} \tag{2.31}$$

$$v_{0s} = R_s i_{0s} + p \lambda_{0s} \tag{2.32}$$

$$v'_{qr} = R'_r i'_{qr} + (\omega - \omega_r) \lambda'_{dr} + p \lambda'_{qr} \tag{2.33}$$

$$v'_{dr} = R'_r i'_{dr} - (\omega - \omega_r) \lambda'_{qr} + p \lambda'_{dr} \tag{2.34}$$

$$v'_{0r} = R'_r i'_{0r} + p \lambda'_{0r} \tag{2.35}$$

Substituting the (2.29) to (2.30)-(2.35) yields the expression for the voltages in terms of the currents, which is shown in matrix form below.

$$\begin{bmatrix} v_{qs} \\ v_{ds} \\ v_{0s} \\ v'_{qr} \\ v'_{dr} \\ v'_{0r} \end{bmatrix} = \begin{bmatrix} R_s + pL_{ss} & \omega L_{ss} & 0 & pL_M & \omega L_M & 0 \\ -\omega L_{ss} & R_s + pL_{ss} & 0 & -\omega L_M & pL_M & 0 \\ 0 & 0 & R_s + pL_{ss} & 0 & 0 & 0 \\ pL_M & (\omega - \omega_r)L_M & 0 & R'_r + pL'_{rr} & (\omega - \omega_r)L'_{rr} & 0 \\ -(\omega - \omega_r)L_M & pL_M & 0 & -(\omega - \omega_r)L'_{rr} & R'_r + pL'_{rr} & 0 \\ 0 & 0 & 0 & 0 & 0 & R'_r + pL'_{rr} \end{bmatrix} \cdot \begin{bmatrix} i_{qs} \\ i_{ds} \\ i_{0s} \\ i_{qr} \\ i_{dr} \\ i_{0r} \end{bmatrix}$$

(2.36)

where

$$L_{ss} = L_{ls} + L_M \tag{2.37}$$

$$L'_{rr} = L'_{lr} + L_M \tag{2.38}$$

To state the electromagnetic torque in terms of the arbitrary reference-frame variables, the equations of the Park's transformation must be substituted in (2.21) as follows.

$$T_e = \left(\frac{P}{2}\right)\left(K_s^{-1} i_{dq0s}\right)^T \frac{\partial}{\partial \theta_r} L'_{sr} (K_r^{-1} i'_{dq0r}) \tag{2.39}$$

Therefore the expression of the torque equation in terms of dq-axis components currents is as follows.

$$T_e = \frac{3}{2}\frac{P}{2} L_M (i_{qs} i'_{dr} - i_{ds} i'_{qr}) \tag{2.40}$$

2.5 Steady state analysis

In this section, the steady state operation of the induction machine is considered and the related equations will be derived using the transient model. Since the steady state model is often expressed in terms of reactances, the machine equations should be modified and expressed in terms of reactances at frequency of ω_b, which generally corresponds to the rated or base frequency of the machine. Therefore the flux equations will be modified as follows.

$$\begin{aligned}
\psi_{qs} &= \left(X_{ls} + X_M\right)\cdot i_{qs} + X_M i'_{qr} \\
\psi_{ds} &= \left(X_{ls} + X_M\right)\cdot i_{ds} + X_M i'_{dr} \\
\psi_{qr} &= \left(X'_{lr} + X_M\right)\cdot i'_{qr} + X_M i_{qs} \\
\psi_{dr} &= \left(X'_{lr} + X_M\right)\cdot i'_{dr} + X_M i_{ds}
\end{aligned} \tag{2.41}$$

Where $X_x = \omega_b L_x$ and $\psi_x = \omega_b \lambda_x$.

When an induction machine is supplied by symmetrical and sinusoidal waveforms and is operating under steady state condition, the zero quantities of the rotor and stator equations are zero and the dq-axis components are constant in a synchronously rotating reference frame; i.e. a reference frame in which $\frac{d\theta}{dt} = \omega_e$ and ω_e is the stator voltage frequency. Therefore, the phase voltages and currents become phasors at the frequency ω_e. For example for three phase balanced stator voltages

$$v_{as} = V_m \cos(\omega_e t + \theta) \tag{2.42}$$

$$v_{bs} = V_m \cos(\omega_e t + \theta - \frac{2\pi}{3})$$

$$v_{cs} = V_m \cos(\omega_e t + \theta + \frac{2\pi}{3})$$

The dq-axis components of the stator voltage in synchronously rotating reference frame are as follows.

$$\begin{aligned} v_{qs} &= V_m \cos(\theta) \\ v_{ds} &= -V_m \sin(\theta) \end{aligned} \tag{2.43}$$

which implies that

$$V_{as} = V_m \angle \theta = V_{qs} - jV_{ds} \tag{2.44}$$

Similarly the rotor voltage phasor is

$$V_{ar} = V_{dr} - jV_{dr} \tag{2.45}$$

Considering the stated points, the voltage equations can be expressed in synchronously rotating reference frame to neglect the time rate of change of all currents. Therefore, the equations for the dq-axis components of the voltages are modified as shown below [18].

$$\begin{aligned} V_{qs} &= R_s I_{qs} + \frac{\omega}{\omega_b} X_{ls} I_{ds} + \frac{\omega}{\omega_b} X_M I_{ds} + \frac{\omega}{\omega_b} X_M I_{dr} \\ V_{ds} &= R_s I_{ds} - \frac{\omega}{\omega_b} X_{ls} I_{qs} - \frac{\omega}{\omega_b} X_M I_{qs} - \frac{\omega}{\omega_b} X_M I_{qr} \end{aligned} \tag{2.46}$$

$$V_{qr} = R_r I_{qr} + \frac{(\omega - \omega_r)}{\omega_b} X_{lr} I_{dr} + \frac{(\omega - \omega_r)}{\omega_b} X_M I_{dr} + \frac{(\omega - \omega_r)}{\omega_b} X_M I_{ds} \tag{2.47}$$

$$V_{dr} = R_r I_{dr} - \frac{(\omega - \omega_r)}{\omega_b} X_{lr} I_{qr} - \frac{(\omega - \omega_r)}{\omega_b} X_M I_{qr} - \frac{(\omega - \omega_r)}{\omega_b} X_M I_{qs}$$

Substituting (2.46) into (2.44) and (2.47) into (2.45), the phase quantity phasors can be developed as follows.

$$V_{as} = \left(R_s + j \frac{\omega_e}{\omega_b} X_{ls} \right) I_{as} + j \frac{\omega_e}{\omega_b} X_M \left(I_{as} + I_{ar} \right) \tag{2.48}$$

$$V_{ar} = \left(\frac{R_r}{s} + j \frac{\omega_e}{\omega_b} X_{lr} \right) I_{ar} + j \frac{\omega_e}{\omega_b} X_M \left(I_{ar} + I_{as} \right) = 0 \tag{2.49}$$

In (2.49), s is known as the slip and is calculated as in (2.50).

$$s = \frac{(\omega_e - \omega_r)}{\omega_e} \tag{2.50}$$

The equivalent circuit that represents the steady state operation of the machine is shown in Figure 2-3. Since ω_b and ω_e are both given explicitly and ω_b corresponds to rated frequency, which is usually used to calculate per unitized reactances, this equivalent circuit is valid for steady state operation in any frequency.

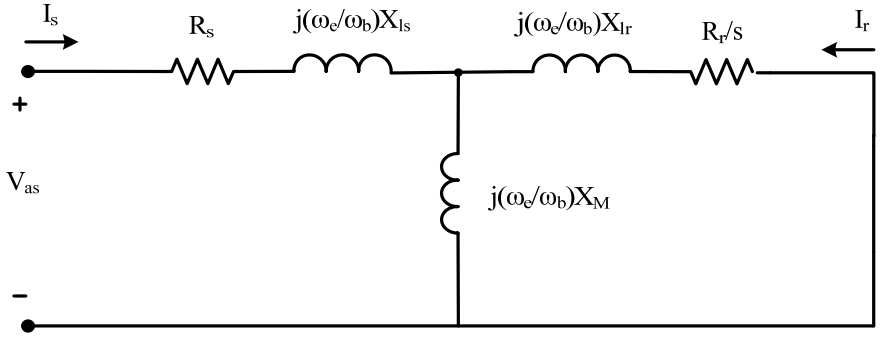

Figure 2-3 Equivalent circuit of the machine in sinusoidal steady state

Chapter 3

Circuitry for AC Machine Control

A modern electric motor drive is a complex power-electronic system that is used to interface an electric motor with the utility grid (or other source of power) to adjust the input parameters of the motor, e.g. terminal voltage, frequency or current. The aim of a drive system is to control one or more of the outputs of the machine, e.g. position, speed or torque by strategically adjusting some of its inputs. Motor drives come in a variety of forms and have varying levels of complexity depending on their intended use. In this chapter, a widely-used drive circuit, which connects an ac source with fixed parameters (frequency and voltage) to an ac motor via an intermediate dc link is presented and discussed. This circuit allows creation of an ac voltage with controllable quantities at the terminals of an ac machine. The same circuit can be used in a variety of motor drive applications depending on the adopted control algorithm and how its individual modules are operated. In the sections that follow each power conversion stage of this circuit is explained in detail, with focus on inversion and its functional operation [2], [4], [18].

3.1 System topology

As previously stated, the objective of an ac drive system is to enable the motor to match the requirement of the load precisely by adjusting the electrical inputs to the motor. The electrical voltage of the utility grid has fixed frequency and magnitude; therefore a drive circuit is used to convert them into controlled variable waveforms. In order to accomplish this conversion process, the electrical power must pass through three stages: rectification (conversion from ac to dc), storage (to absorb energy flow fluctuations), and inversion (conversion from dc to ac). Figure 3-1 shows this process.

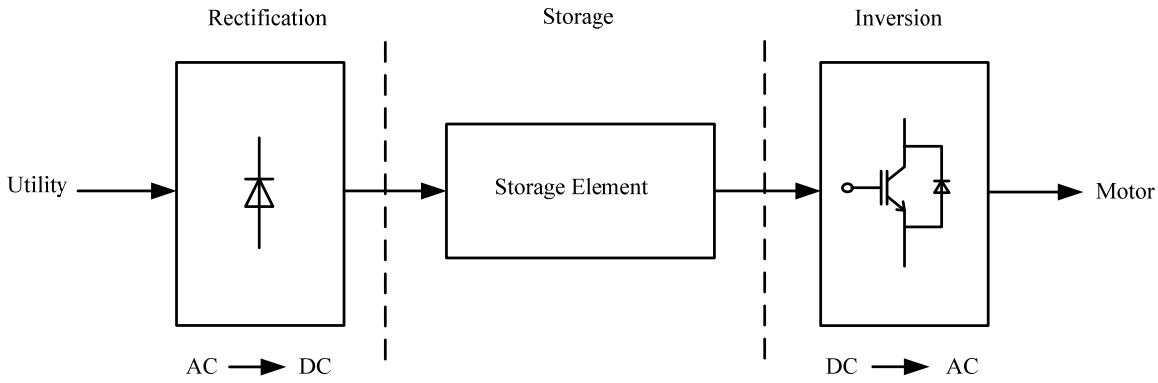

Figure 3-1 Power processing stages

In the rectifier stage, power semiconductor devices are used to convert the ac quantities of the utility grid to a nearly constant dc waveform. Then in the next stage the converted energy should be stored in an intermediate storage element, which is usually a capacitor, an inductor or a combination of both. In the final stage of inversion, power semiconductor devices are utilized to convert the stored energy into a suitable form to match the desired operating conditions of the electric motor.

3.2 Rectifiers

The rectifier is a power electronic device that consists of semiconductor switches to convert ac waveforms to dc. Therefore, in the first stage of power processing of an ac drive, a rectifier is utilized. Several topologies for rectifiers exist, which have their own merits and disadvantages. Depending on the type of semiconductor switches used rectifiers can be classified as controllable or uncontrollable. In this thesis, the purpose is to control the voltage and frequency of the motor by controlling the inverter output; hence a simple three phase diode bridge rectifier (also referred to as an uncontrolled six-pulse rectifier) is considered as the ac/dc converter of the drive.

The use of uncontrollable diodes eliminates the control over the dc bus voltage. Diode front-end drives need provisions to reduce their impact on the harmonic content of their ac-side current. Despite this disadvantage, they are still widely used in many applications because of their simple structure, absence of control, and low cost. This is particularly true in medium power drive applications [20], [21].

Figure 3.2 shows the schematic diagram of a three-phase diode bridge. The figure also shows a model of the input ac system consisting of an *RL* series impedance.

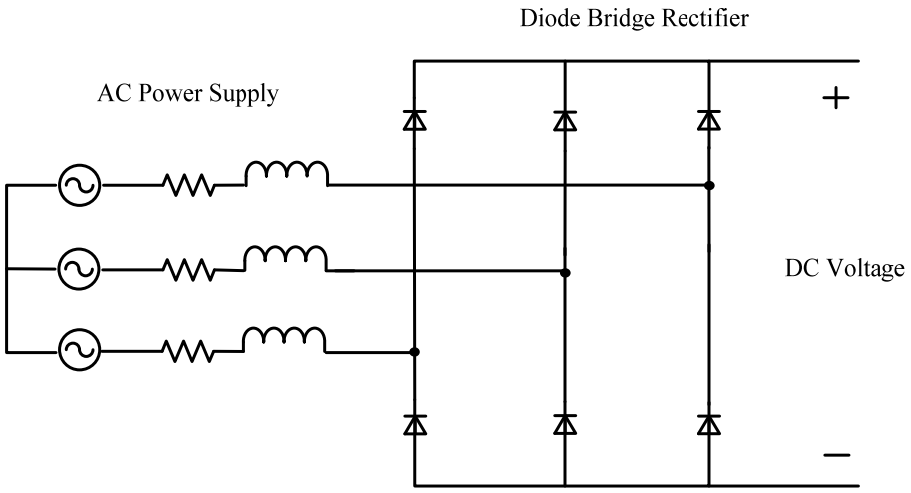

Figure 3-2 Three phase diode bridge rectifier

3.3 Storage

For the intermediate stage of the considered drive system, an inductive-capacitive (LC) combination is employed. The capacitor is to store the energy passed from the utility grid. The LC also operates as a low pass filter to further suppress the dc ripple and provide nearly constant dc voltage for the following stage of inversion. Larger values of the L and C improve the steady state performance; however, it has undesirable effects on the transient response.

In the case of regenerative braking, the energy has to go back from inverter. However the diode bridge that is used as the first stage of the drive system is unidirectional, and cannot transfer the energy to the utility grid. Consequently, the energy will be absorbed by the capacitor and it causes the voltage of the capacitor to increase significantly. This event can have destructive effects on the capacitor. Therefore a bypass circuit should be

employed to avoid dc link over-voltage by dissipating the energy from the regenerative braking action.

This bypass circuit consists of a controlled switch and a resistor in parallel with the capacitor. Figure 3-3 shows the switching strategy used for this part of circuit. When the voltage across the capacitor increases, the variable duty cycle of the series switch will increase accordingly to provide the current path through the resistor to dissipate the excessive energy, and hence prevent over-voltage [22].

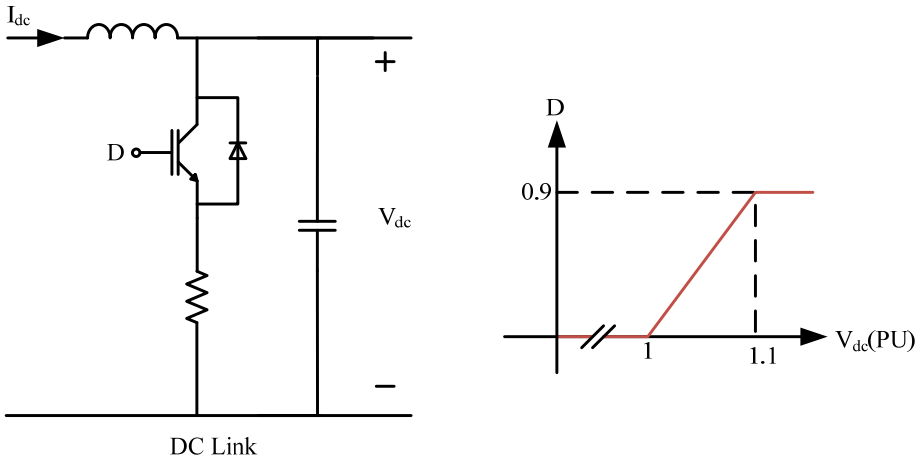

Figure 3-3 dc link circuit

3.4 Inverters

The inverter is built using switching devices that convert the rectified dc voltage into variable frequency, variable amplitude ac waveforms that are suited for adjusting the input parameters of the ac electric machines. Depending on the type of the supply source and the adopted topology of the power circuit, inverters are classified as voltage source inverters (VSI) and current source inverters (CSI).

The main issue associated with inverters is that the output voltage is never purely sinusoidal, and by controlling the fundamental component of the output voltage, one can obtain a controlled input voltage for the machine. The quality of the waveforms, however, depends on different method of the switching. Here, first the inverter of the ac drive, which is a three phase two level VSI and its functional operation is discussed. Then the concept of switching function and the sinusoidal PWM in three phase VSIs are explained [20], [21].

3.4.1 Two-level three-phase VSI and switching function

Figure 3-4 shows one leg of a two level VSI. Upper and lower switches cannot have the same state simultaneously, because turning on both switches at the same time causes a short circuit of the dc voltage and turning both off leads to an open circuit that may interrupt the load current. Depending on the states of the switches, two voltage levels at the output are obtained. In order to allow bi-directional current flow, the anti parallel diodes are used.

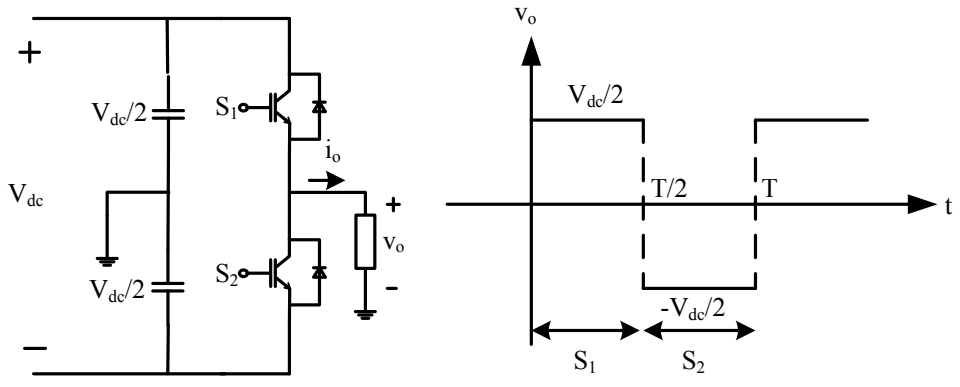

Figure 3-4 One leg of a two level VSI and the output voltage

For three phase operation, three identical legs are used. The main purpose is to generate a set of voltages that are displaced by 120º and have equal magnitude and frequency. Therefore each leg receives a gate pulse displaced by 120º from the previous leg.

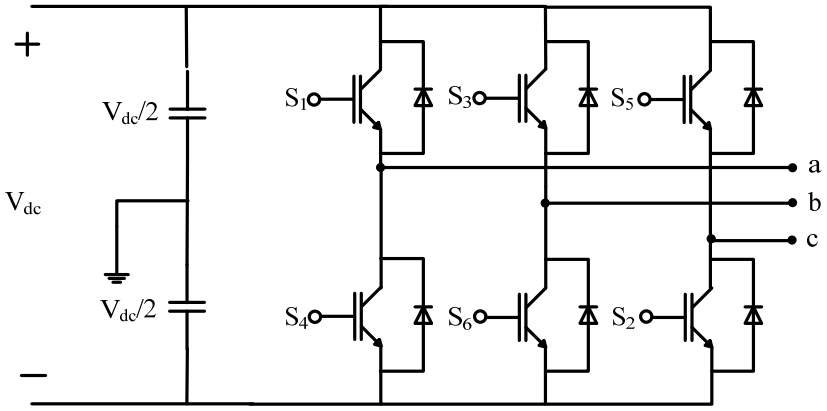

Figure 3-5 Two-level three-phase voltage source inverter

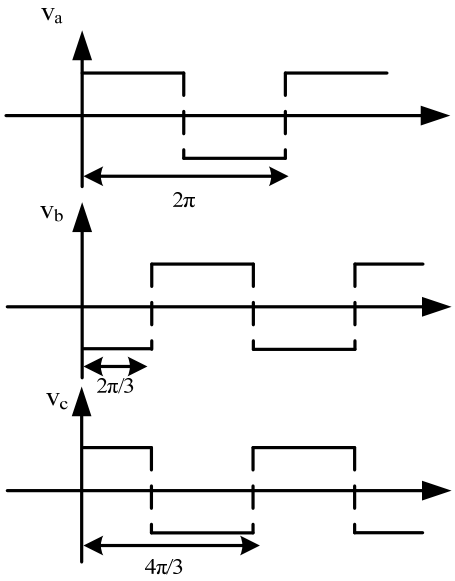

Figure 3-6 Output voltages of a three-phase VSI

This mode of operation of the switching cell is known as square wave operation. Although this operation is not complicated and has low switching losses, its major disadvantage is that under this regime the only parameter that can be changed to control the fundamental component magnitude is the dc link voltage, which is not a suitable solution. Also the generated waveform has significant low frequency harmonics, so the quality of the output voltage is not desirable in this technique.

Pulse width modulation (PWM) is a waveform generation scheme that overcomes the problem of the square wave operation. This technique is based on fast switching of controlled switches with variable durations in such a way that the fundamental component of the generated output has the desired magnitude and phase. There are several modulation methods including sinusoidal PWM (SPWM), selective harmonic elimination (SHE) and space vector modulation (SVM), to name a few [23]-[25].

SPWM is one of the most popular switching schemes that is used to control the output voltage of the inverter in ac drives. In this method the waveform generation is based on comparison of a fundamental frequency sinusoidal reference with a high-frequency triangular carrier waveform, as depicted in Figure 3-7 for one leg of a VSI. SPWM controls each leg of the VSI independently of other length. A three phase SPWM generator has three separate comparators with equal carrier but reference waveforms with 120º phase shift to generate symmetrical three phase output.

The modulation index is defined as the ratio of the amplitude of the reference signal over the carrier signal. It can be proven that the modulation index can directly controls

the amplitude of the fundamental component and their relationship is linear as long as it varies over the interval $[0,1]$ as shown in [26].

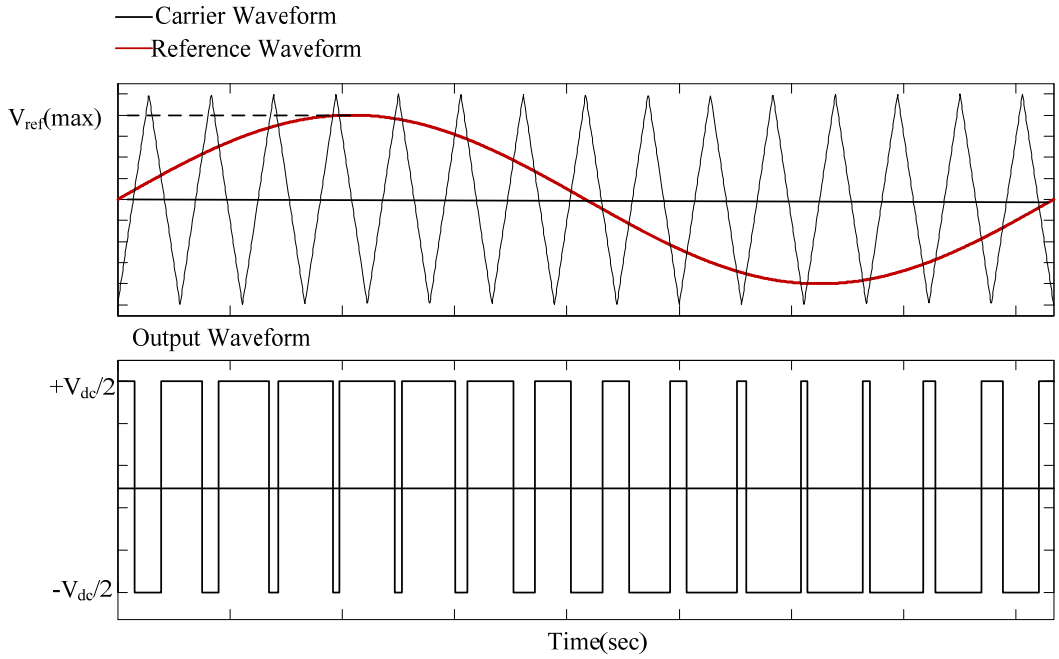

Figure 3-7 Sinusoidal pulse width modulation

The number of switching actions in one cycle is defined by the frequency ratio $n = f_c / f_{ref}$. In case of three phase operation, this number should be selected to be odd and a multiple of three, since odd number results in waveform generation that has quarter-cycle symmetry, and a multiple of three eliminates triple-*n* harmonics in a balanced three-phase system. Figure 3-8 illustrates the harmonic spectrum of the voltage waveform shown in Figure 3-7 with a frequency ratio of $n = 15$. It can be observed that the harmonic contents are mostly around n , $2n$, etc, and also even harmonics are eliminated due to the odd ratio of the frequencies.

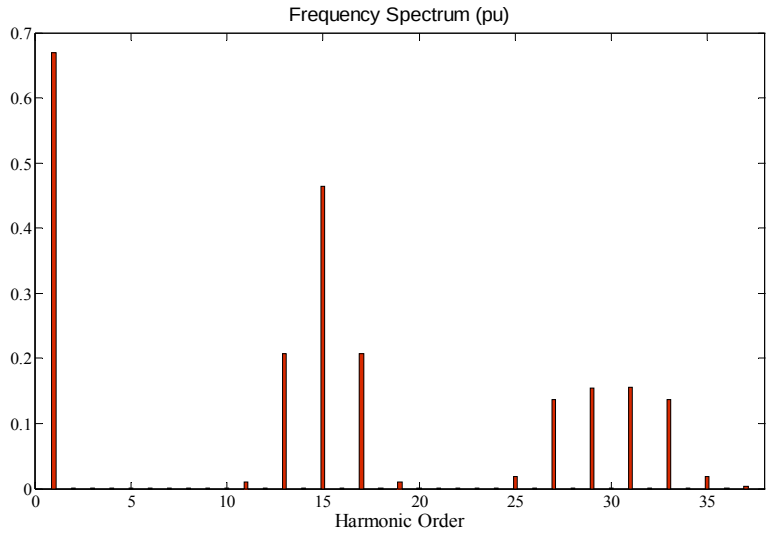

Figure 3-8 The harmonic spectrum of the voltage waveform (Figure 3-7) with a frequency ratio of n=15

Considering the drive system described in this chapter, the voltage at the terminals of the motor can be controlled by appropriate selection of firing pulses of VSI switches. In the following chapters control methodologies that determine the reference voltage for desirable operation of the induction machine will be presented. Once the reference voltage is obtained the SPWM technique is applied to properly find the firing pulse.

Chapter 4

Vector Controlled Induction Motor Drives

Induction machine drives can be broadly categorized into steady state-based and dynamics-based drives. In the former, observations drawn from steady state operation of the machine are used to form a strategy for its drive. Not surprisingly these drives perform satisfactorily in steady state, but their transient performance cannot be predicted or controlled precisely. In the latter category, i.e. dynamics-based drives, a mathematical model of the machine that is valid in both transient and steady state is used to develop strategies for drive. As such these drives provide superior performance, albeit at the cost of more complexity of the algorithm. In this chapter, attention will be paid to the dynamics-based drive strategies for induction machines.

Considering the dynamic response of a steady state-based drive, the reason for the poor (or unpredictable) dynamic response is the deviation of the air gap flux linkages from their set values. This deviation is not only in magnitude but also in phase.

Oscillations in the air gap flux linkages result in oscillations in the electromagnetic torque, and left unattended, result in speed oscillations. This is undesirable in many high-performance applications where high precision, fast positioning, or tight speed control are required [5].

A large class of dynamics-based induction machine drives are called the field-oriented control or vector control methodologies. The main purpose of them is to implement a control scheme in which the electromagnetic torque can follow the reference torque command nearly instantaneously to produce high quality dynamic performance in terms of response times [5],[27]-[31].

They use the transient model of the machine and aim to replicate the desirable features of control of a separately-excited dc machine, in which the armature and field currents can independently control the torque and field flux of the machine, while maintaining the ideal perpendicularity of the two fluxes. This is far more difficult to achieve in an ac machine, and requires a coordinated control of the stator current magnitudes, frequencies, and their phases. If the stator current phasor is resolved onto the rotor flux linkages, its component along the rotor flux linkages is the field producing current; this however requires the position of the rotor flux linkages at every instant, and unlike dc machines it is a dynamically varying quantity. If this is available then the control of the ac machine becomes similar to that of a separately excited dc machine. The requirement of the phase, frequency and magnitude control of the currents and hence of the flux phasor is made possible by inverter control.

Vector control has made the ac drives equivalent to dc drives because of the independent control of the flux and torque and consequently in their dynamic

performance. These developments positioned the ac drives for high performance applications.

In this chapter, first the basic principles and modeling of the most prevalent type of vector control schemes, i.e. direct vector control and indirect vector control, will be described. Then the implementation and optimization of indirect vector control of an induction machine will be discussed. At the end of the chapter the simulation results will be presented.

4.1 Principles of vector control

In an induction motor, the stator current i_s produces both the rotor flux λ_r and the electromagnetic torque T_e. In other words, the stator current has two components i_f and i_T that

$$\lambda_r \propto i_f \tag{4.1}$$

$$T_e \propto \lambda_r i_T \tag{4.2}$$

The principle of the vector control is explained by assuming that the position of the rotor flux linkages space vector λ_r is known. In the following presentation, the field angle θ_f is the angular position of the rotor field in a stationary reference frame attached to the stator. The dq-axis components of the stator current in reference frame attached to θ_f are i_{qs}^e and i_{ds}^e [5]. Using Park's transformation

$$\begin{bmatrix} i_{qs}^{e} \\ i_{ds}^{e} \end{bmatrix} = \frac{2}{3}\begin{bmatrix} \cos\theta_f & \cos\left(\theta_f - \frac{2\pi}{3}\right) & \cos\left(\theta_f + \frac{2\pi}{3}\right) \\ \sin\theta_f & \sin\left(\theta_f - \frac{2\pi}{3}\right) & \sin\left(\theta_f - \frac{2\pi}{3}\right) \end{bmatrix} \cdot \begin{bmatrix} i_{as} \\ i_{bs} \\ i_{cs} \end{bmatrix} \tag{4.3}$$

The component of the stator current that produces the rotor flux has to be in phase with λ_r. Using Park's transformation in the synchronous reference frame, the stator current component i_{ds}^{e} that is along the λ_r should be the field producing component (i_f), and the perpendicular component i_{qs}^{e} is hence the torque producing component (i_T). The phasor diagram of the vector control is as shown in Figure 4-1 [5].

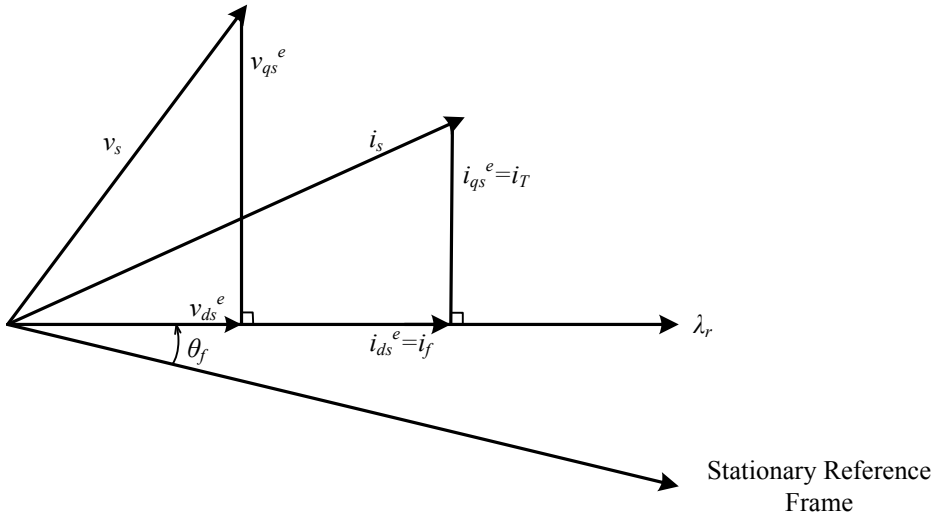

Figure 4-1 Phasor diagram of the vector control

In this reference frame the dq-axis components of the rotor flux linkages are:

$$\lambda_{qr}^{'e} = 0 \tag{4.4}$$

$$\lambda_{dr}^{'e} = L_{rr}^{'} i_{dr}^{'e} + L_M i_{ds}^{e} \tag{4.5}$$

Now consider the d-axis rotor voltage equation

$$R_r^{'} i_{dr}^{'e} - (\omega_e - \omega_r)\lambda_{qr}^{'e} + p\lambda_{dr}^{'r} = 0 \tag{4.6}$$

Substituting (4.4) and (4.5) into (4.6) yields

$$R_r^{'} i_{dr}^{'e} + \frac{d}{dt}\left(L_{rr}^{'} i_{dr}^{'e} + L_M i_{ds}\right) = 0 \tag{4.7}$$

Or

$$R^{'}{}_r i_{dr}^{'e} + L_{rr}^{'} \frac{d}{dt} i_{dr}^{'e} = -\frac{d}{dt} L_M i_{ds} \tag{4.8}$$

Considering (4.8), if the d-axis stator current is kept constant in order to adjust the field at a given value then d-axis rotor flux tends to zero.

$$i_{dr}^{'e} = 0 \tag{4.9}$$

Therefore substituting (4.4) and (4.9) in the rotor flux equation in synchronous reference frame gives $i_{qr}^{'e}$ and i_{ds}^{e}

$$i_{qr}^{'e} = -\frac{L_M}{L_{rr}^{'}} i_{qs}^{e} \tag{4.10}$$

$$i_{ds}^{e} = \frac{1}{L_M} \lambda_{dr}^{'e} \tag{4.11}$$

Now by using the rotor and stator current equations, the torque equation can be expressed in terms of the rotor flux linkages and torque producing component of the stator current as follow.

$$T_e = \frac{3}{2}\frac{P}{2}\frac{L_M}{L_{rr}} \lambda_{dr}^{'e} i_{qs}^{e} \tag{4.12}$$

In vector control by controlling the direct-axis component of the stator current in synchronous reference frame (which is the flux producing component), the rotor flux

linkages are controlled. In essence it is similar to separately excited dc machines. Then from the λ_r^* and the required torque T_e^*, the torque producing component of the stator current can be calculated. Controlling the torque producing component of the stator current when the rotor flux linkages phasor is constant gives an independent control of the electromagnetic torque. Note that the only matter here is how to achieve the position of the synchronous reference frame, which is attached to the rotor flux.

Vector control schemes are classified according to how the rotor field position is acquired. If the flux angle is calculated by using terminal voltages and currents or Hall sensors or flux sensing windings, then it is known as the direct vector control. If the field angle is obtained by using rotor position measurement and partial estimation with only machine parameters, it leads to a class of control schemes known as the indirect vector control [5].

The direct and indirect vector control principles are explained in the following sections. However, in this thesis the indirect vector control for the induction motor is employed, so further discussions on the vector control scheme will emphasize the indirect vector control and the implementation results will be presented.

4.1.1 Direct vector control

The underlying idea of the direct vector control is to use flux measurements to estimate the rotor flux linkages in the stationary reference frame and then determine the position of the synchronous reference frame wherein the d-axis of the reference frame is aligned with the $\lambda_r^{'}$ [18].

In this method, Hall effect sensors are located in a stationary reference frame in the air gap and are used to measure the air gap flux in the d and q-axis, λ^s_{qm} and λ^s_{dm} , of the stationary reference frame. Using λ^s_{qm} and λ^s_{dm} and the machine parameters, λ'^s_{qr} and λ'^s_{dr} can be estimated by the following equations.

Note that

$$\lambda^s_{qm} = L_M\left(i^s_{qs} + i'^s_{qr}\right) \tag{4.13}$$

Therefore,

$$i'^s_{qr} = \frac{\lambda^s_{qm}}{L_M} - i^s_{qs} \tag{4.14}$$

Also the q-axis rotor flux linkages may be expressed as

$$\lambda'^s_{qr} = (L'_{lr} + L_M)i'^s_{qr} + L_M i^s_{qs} \tag{4.15}$$

Substituting (4.14) into (4.15) yields

$$\lambda'^s_{qr} = \frac{L'_{rr}}{L_M}\lambda^s_{qm} - L'_{lr} i^s_{qs} \tag{4.16}$$

Performing an identical derivation for the d-axis yields

$$\lambda'^s_{dr} = \frac{L'_{rr}}{L_M}\lambda^s_{dm} - L'_{lr} i^s_{ds} \tag{4.17}$$

In this stage, the values of dq-axis components of the rotor flux linkages in the stationary reference frame are used to calculate the position of the synchronous reference frame. The rotor flux components in synchronous reference frame are obtained by equation (4.18) assuming the position of the stationary reference frame is zero.

$$\begin{bmatrix} \lambda'^{e}_{qr} \\ \lambda'^{e}_{dr} \end{bmatrix} = \begin{bmatrix} \cos\theta_e & -\sin\theta_e \\ \sin\theta_e & \cos\theta_e \end{bmatrix} . \begin{bmatrix} \lambda'^{s}_{qr} \\ \lambda'^{s}_{dr} \end{bmatrix} \tag{4.18}$$

Now to align the rotor flux linkage with the d-axis of the synchronous reference frame, the position of the synchronous reference frame should be defined as

$$\theta_e = angle\left(\lambda'^{s}_{qr} - j\lambda'^{s}_{dr}\right) + \frac{\pi}{2} \tag{4.19}$$

Also note that the magnitude of the flux in any reference frame is the same

$$\lambda'^{e}_{dr} = \sqrt{\left(\lambda'^{s}_{qr}\right)^2 + \left(\lambda'^{s}_{dr}\right)^2} \tag{4.20}$$

Once the angle θ_e is determined the remainder of the drive strategy is as outlined in section 4.1.

4.1.2 Indirect vector control

Using Hall-effect sensors to sense the air gap flux in direct field control is expensive in practice since positioning the flux sensors requires special modifications of the motor. Moreover, using the sensed signal to calculate the rotor flux may lead to inaccuracies due to variations in the flux level and temperature. Therefore indirect vector control has captured more interests in field oriented control methods. Indirect vector control requires an estimation of machine parameters to obtain the field angle. Although it alleviates the problems associated with the direct vector method, it is known to be sensitive to the variations in the machine parameters, in particular the rotor resistance [32], [33].

The indirect vector control is derived from the dynamic equations of the induction machine in the synchronously rotating reference frame and sensing of the rotor flux

linkages is not required in this method. In order to create the algorithm it is useful to first establish the electrical frequency that is utilized in direct field oriented control [5], [18]. The rotor equations of the induction machine containing flux linkages as variables are given by

$$R_r' i_{qr}'^e + (\omega_e - \omega_r)\lambda_{dr}'^e + p\lambda_{qr}'^e = 0 \tag{4.21}$$

$$R_r' i_{dr}'^e - (\omega_e - \omega_r)\lambda_{qr}'^e + p\lambda_{dr}'^e = 0 \tag{4.22}$$

$$\lambda_{qr}'^e = L_{rr} i_{qr}'^e + L_M i_{qs}'^e \tag{4.23}$$

$$\lambda_{dr}'^e = L_{rr} i_{dr}'^e + L_M i_{ds}'^e \tag{4.24}$$

The resultant rotor flux linkage is assumed to be on direct axis, to reduce the number of variables in the equations. Hence, aligning the d-axis with rotor flux phasor yields

$$\begin{aligned} \lambda_{dr}'^e &= \lambda_r' \\ \lambda_{qr}'^e &= 0 \end{aligned} \tag{4.25}$$

Substituting the rotor flux linkage dq-axis components from equation (4.25) in (4.21):

$$\omega_e = \omega_r - R_r' \frac{i_{qr}'^e}{\lambda_r'^e} \tag{4.26}$$

The quadrature component of the rotor currents in terms of the stator currents are derived from (4.23) and (4.25) as

$$i_{qr}'^e = -\frac{L_M}{L_{rl}} i_{qs}'^e \tag{4.27}$$

Note that the torque is proportional to the product of the rotor flux linkages and the stator q-axis current. If the rotor flux is maintained constant, then the torque is simply proportional to the torque producing component of the stator current, as in the case of the

separately excited dc machine with armature current control, where the torque is proportional to the armature current when the field current is constant. Moreover, it was proven that if the d-axis stator current is kept constant in order to adjust the field at a given value then d-axis rotor current tends to zero. Therefore the equation (4.24) will become:

$$\lambda_r^{'e} = L_M i_{ds}^{'e} \tag{4.28}$$

Substituting the rotor flux linkage from (4.28) and the $i_{qr}^{'e}$ from (4.27) in equation (4.28), the synchronous speed is derived in terms of the dq-axis components of the stator current as follows.

$$\omega_e = \omega_r + \frac{R_r^{'}}{L_{lr} + L_M} \frac{i_{qs}^e}{i_{ds}^e} \tag{4.29}$$

The ω_e derived above can be integrated over time to obtain the position of the synchronous reference frame. It can be shown that the initial angle will have decaying effect on the performance of the system and therefore can be set to zero.

$$\theta_e = \int \omega_e dt \tag{4.30}$$

4.2 Implementation of an indirect vector control

The indirect vector controller only measures the speed from the machine while all other parameters are estimated. The torque command (T^*) is generated as a function of speed error signal, generally processed through a proportional-integral (PI) controller.

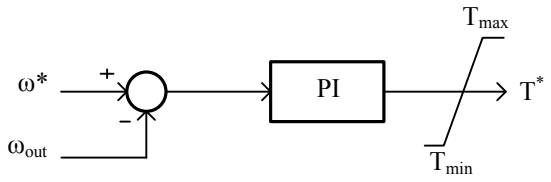

Figure 4-2 Speed controller

The flux command for a simple drive strategy is made to be a function of speed, defined by (4.31).

$$\begin{aligned} \lambda_r^* &= \lambda_b \qquad 0 \le |\omega_r| \le \omega_b \\ \lambda_r^* &= \frac{\omega_b}{|\omega_r|}\lambda_b \qquad \omega_b \le |\omega_r| \le \omega_{r(\max)} \end{aligned} \tag{4.31}$$

where λ_b and ω_r are the rated or the base rotor flux linkages and rotor speed respectively. ω_b is the speed at which the motor runs with full-line voltage applied to the armature and the field. The flux is kept at rated value up to the rated speed. Above that the flux is weakened to maintain the power output at a constant value.

Therefore the desired component of the stator current in terms of the desired torque and flux are

$$\begin{aligned} i_{ds}^{e*} &= \frac{\lambda_r^*}{L_M} \\ i_{qs}^{e*} &= \frac{4L_{rr}^{'}}{3PL_mL_M}\frac{T^*}{\lambda_r^*} \end{aligned} \tag{4.32}$$

Furthermore, the slip speed should be

$$\omega_s = \frac{R_{rr}^{'}}{L_{rr}^{'}}\frac{i_{qs}^{e*}}{i_{ds}^{e*}} \tag{4.33}$$

Figure 4-3 summarizes the process of generating three phase stator current commands

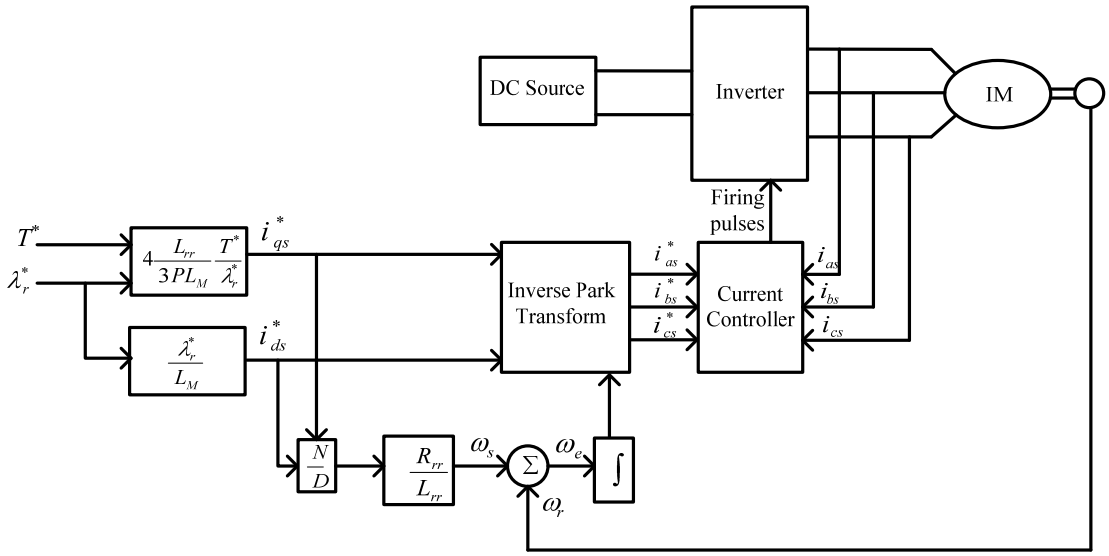

Figure 4-3 Indirect vector control scheme

In the above discussion the dc/ac converter is assumed to be a current source inverter and through hysteresis controllers the phase currents are regulated, but in this thesis a voltage source inverter is used as the last stage of the ac drive therefore the generated currents should be converted into voltages to be given to the voltage source converter as the reference voltages.

4.2.1 Voltage Decoupler

In this approach the challenge is that current commands cannot be used directly for controlling the VSI. Therefore, the proper stator voltages V_{ds}^* and V_{qs}^* that will result in the desired stator currents should be generated by means of a feedback loop. The following equations shows the relationship between the stator currents and voltages

$$V_{qs} = R_s i_{qs} + \omega_e L_{ss} i_{ds} + \left(L_{ss} - \frac{L_M^2}{L_{rr}} \right) \frac{d}{dt} i_{qs} \tag{4.34}$$

$$V_{ds} = R_s i_{ds} - \omega_e \left(L_{ss} - \frac{L_M^2}{L_{rr}} \right) i_{qs} + L_{ss} \frac{d}{dt} i_{ds} \tag{4.35}$$

It can be seen that the i_{ds} and i_{qs} are inter-related due to the terms $\omega_e L_{ss} i_{ds}$ and $-\omega_e \left(L_{ss} - \frac{L_M^2}{L_{rr}} \right) i_{qs}$ in the equations (4.34) and (4.35) respectively. A decoupled controller can be used to solve the problem, so that i_{ds} and i_{qs} can be controlled independently.

The implementation of the voltage decoupler is illustrated in Figure 4-4 . Then through inverse Park transformation and then with the proper normalization, the generated voltages can be fed into a sinusoidal PWM unit as reference voltage to control the three phase VSI.

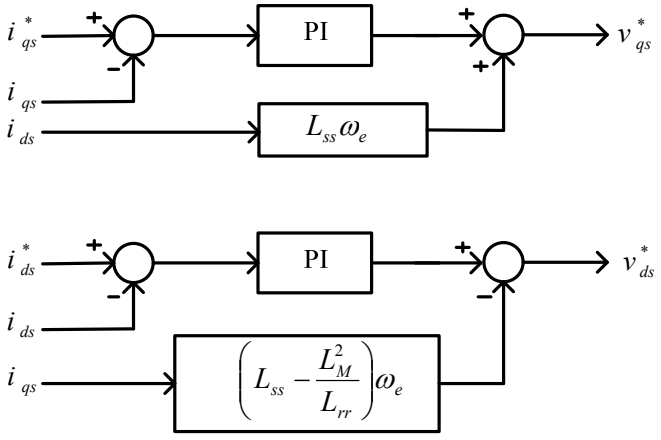

Figure 4-4 Voltage decoupler

4.3 Design goals and simulation based optimal design

When a control system is designed to drive an induction machine, several objectives must be fulfilled according to the machine application. For example, this requires proper selection of the control system parameters as well as values of the inductor and capacitor in the low pass filter portion of the drive circuitry. This thesis proposes the use of simulation-based nonlinear optimization as a means to determine the parameters of the system.

In a drive system, filter elements have a significant impact on final results. Larger elements provide dc voltage and current with better quality in steady state, but they degrade the transient performance. Smaller filter elements improve the transient performance but degrade the steady state response. Therefore, finding the acceptable values for the filter elements needs trade off between two competing objectives, fast transient response and low steady state ripple.

Two other important outputs of the drive system are the torque and the speed. As the output torque and speed of the induction machine are regulated by the controller, the gain and time constant of the PI controllers in the controller should be carefully selected to accomplish the objectives. The indirect vector control for this drive system is chosen to control the speed of the motor. Consequently, it is expected that the control system follows the changes in the reference speed rapidly and with minimum deviation.

Furthermore, in order to have a smooth rotation of the motor's shaft for reducing mechanical stresses, the electrical torque ripple should be minimized.

As mentioned earlier, because of the nonlinear switching structure of the power electronic devices in drive system and complicated nature of the control scheme, an explicit mathematical description of the system is not possible and conventional design methods are not practical; therefore, using a computer simulation model for designing such complex power electronic systems is inevitable. Although by trial and error through several simulations and using engineering judgement, one can acquire the filter elements and the controller parameters that result in stable performance of the system, obtaining optimal results that accomplish the desired objectives is still not feasible by this method. Alternatively a computer simulation model along with nonlinear optimization algorithm can solve the problem of optimal design of such systems [10]-[12].

In this thesis the drive system is implemented in the PSCAD/EMTDC transient simulator. Then the nonlinear simplex optimization method is wrapped around the simulator to intelligently select the parameters. An appropriate objective function, which represents the design expectations, should be developed. In this objective function the following factors are considered:

- Deviation of the actual speed form the set value
- Torque ripple
- dc voltage ripple
- Sizes of L and C

To quantify these aspects of the system performance, the following sub-objective functions are defined to consider the behaviour of the system under transient and steady state conditions.

$$OF_1 = 100\int_{ss}(\omega_{out}-\omega_{ref})^2 + \frac{1}{100}\int_{transient}(\omega_{out}-\omega_{ref})^2 \tag{4.36}$$

$$OF_2 = \int T^2_{elec-Ripple} \tag{4.37}$$

$$OF_3 = \int V^2_{dc-Ripple} \tag{4.38}$$

$$OF_4 = \frac{C_{dc}[\mu F]}{5000} + 500L_{dc}[mH] \tag{4.39}$$

The first sub-objective function expressed in (4.36) calculates the deviation of the reference speed from the actual speed during the transient and steady state periods. The torque ripple of the machine is evaluated by the second sub-objective function (4.37). The third one, expressed in (4.38), calculates the dc link voltage ripple. The sizes of the low pass filter elements are considered by the last sub-objective function stated in (4.39). Since all of the sub-objective function should be satisfied simultaneously, they are combined into one objective function using a linear weighted combination.

$$OF_t\left(G_{Vd},T_{Vd},G_{Vq},T_{Vq},G_{\omega},T_{\omega},L_{dc},C_{dc}\right) = k_1OF_1 + k_2OF_2 + k_3OF_3 + k_1OF_4 \tag{4.40}$$

Selecting a suitable set of weighting factors for sub-objective function is an important step that can be done by performing several experiments to observe the range of variation of each sub-objective function, since the value of the sub-objective functions are not in the same range. Moreover, it requires the prior knowledge about the impact of each sub-

objective function on the other ones. As mentioned earlier, smaller filter elements degrade dc voltage and current in steady state. The weighting factors that are obtained for this sub-objective functions are as follows.

$$K_1 = 250 \quad K_2 = 2000 \quad K_3 = 1500 \quad K_4 = 1 \tag{4.41}$$

These values were obtained through an initial round of experiments with the simulation model. Formal methods such as Pareto optimality to decide the relative weight of the competing sub-objectives exist, where trade-offs can be accurately assessed and weights can be assigned accordingly. These methods are discussed in detail in [10] and may be adopted. Since the objective of this thesis is development of reduced-intensity simulation models for machine drives, an exhaustive process for selecting the weights has been avoided to maintain focus on the optimization process and methods to reduce its computational intensity.

4.4 Simulation case and optimization results

In this project, the PSCAD/EMTDC is used to model the entire system, which consists of the power electronics drive system (as a means of interfacing the induction machine with the utility grid) and the controller system. Figure 4-5 illustrates the detailed model of the drive system with the power electronic switches in the PSCAD/EMTDC along with the decoupled vector control system. Table 4-1 shows the parameters of the drive system.

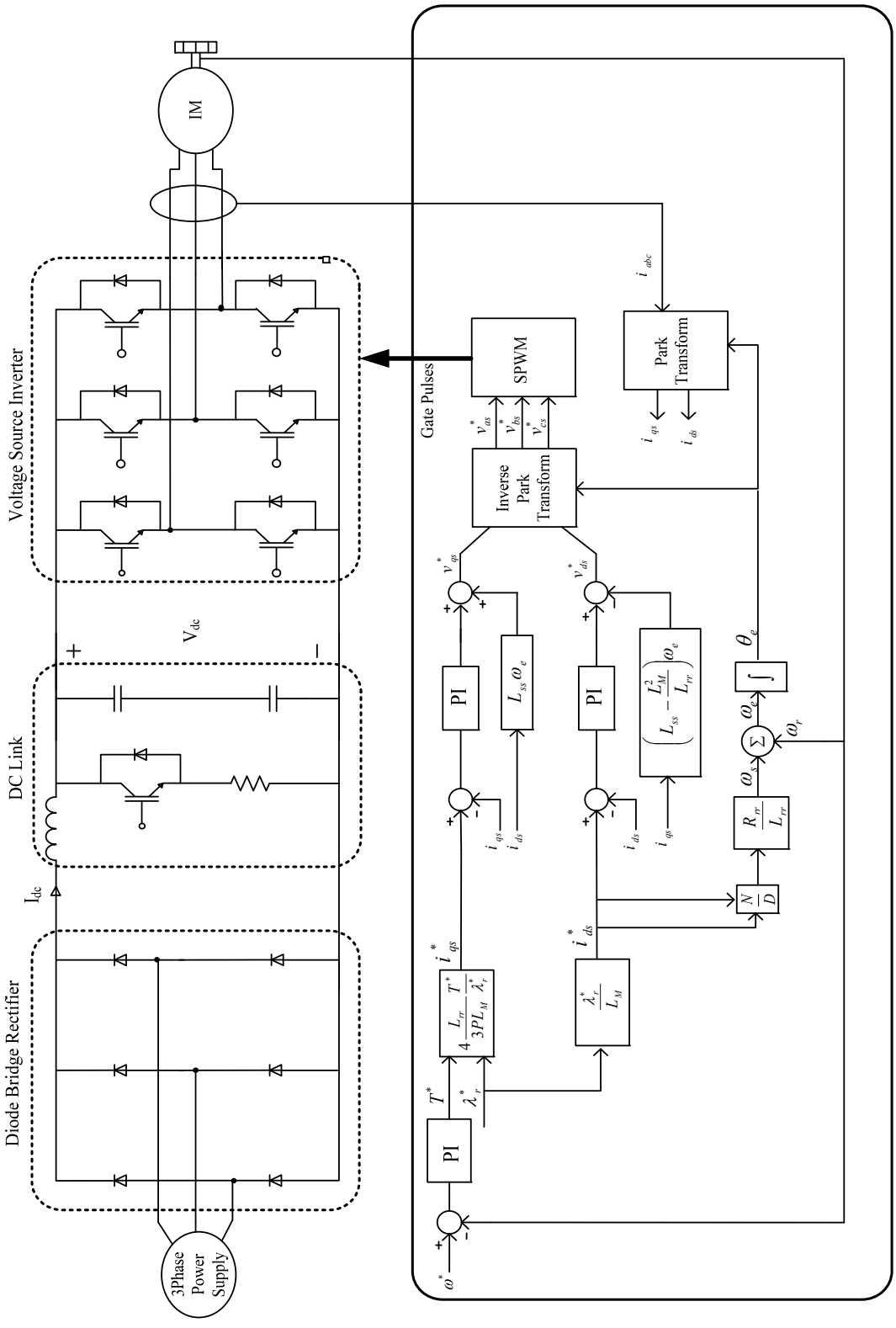

Figure 4-5 Detailed model of the drive system along with the indirect vector controller

Table 4-1 Drive system parameters

	Rated values	
Induction motor	Voltage	2300 [V]
	Power	500 [hp]
	Frequency	60 [Hz]
	J	11.06 [Kg.m^2]
	R_s	0.262
	X_{ls}	1.206
	X_M	54.02
	X_{lr}	1.206
	R_r	0.187
	Pole	4
Input ac system	Voltage	3900 [V]
	Frequency	60 [Hz]

In this drive system, the unknown values are six parameters of the control system G_{Vd}, T_{Vd}, G_{Vq}, T_{Vq}, G_{ω}, T_{ω} and two parameters of the power circuit L_{dc} and C_{dc}. The PSCAD/EMTDC has an optimization tool that uses simplex method with the multi-run feature to find the optimum set of parameters that result in the smallest value of the objective function with minimum human interaction.

In order to evaluate the performance of the drive system precisely, the system operation should be observed during steady state and transient conditions with various motor loads and a wide range of reference speed in one period of simulation. Therefore, the motor is operated under the sequence of conditions depicted in Figure 4-6.

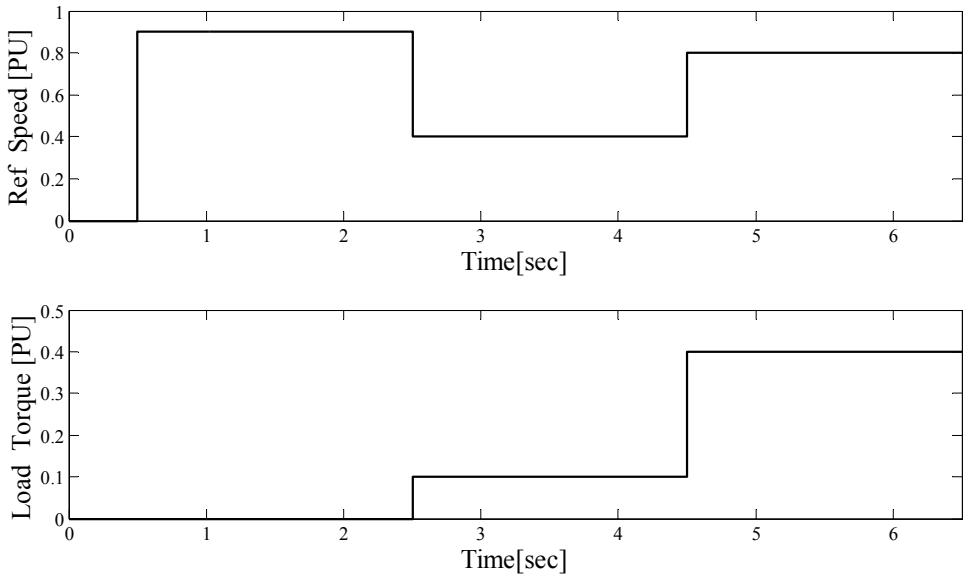

Figure 4-6 Reference speed and load torque variations

After 643 simulations (on a 2.67 GHz, dual core machine) taking 49200.90 seconds (equivalent to 13 hours and 40 minutes), the optimization algorithm finds the optimum point with the minimum (local) value for the objective function. To evaluate the system performance the value of the objective functions after first and the last experiment should be observed to compare the optimal results with the initial results. Table 4-2 present the objective function values along with the corresponding sub-objective functions.

Table 4-2 Objective function values before and after optimization

	OF_1	OF_2	OF_3	OF_4	OF_t
Initial	0.00043441	0.0090903	0.0415532	0.6	189.717
optimum	0.00003808	0.0059501	0.0004833	1.105	23.252

Considering the sub-objective functions in Table 4-2, it can be observed that after optimization the machine transient and steady state performance is improved significantly. The speed error is reduced by nearly one-eleventh and the torque ripple is reduced to approximately half. Initially the size of the filter elements was chosen to be small, but the optimization showed that by increasing the filter size within a reasonable range, considerable improvement in the dc voltage quality is achieved leading to minimization of the torque ripple.

Figure 4-7and Figure 4-8 depict the speed and torque dynamic behaviour of the induction machine under different conditions of the reference speed and variation of the load torque after and before the optimization respectively.

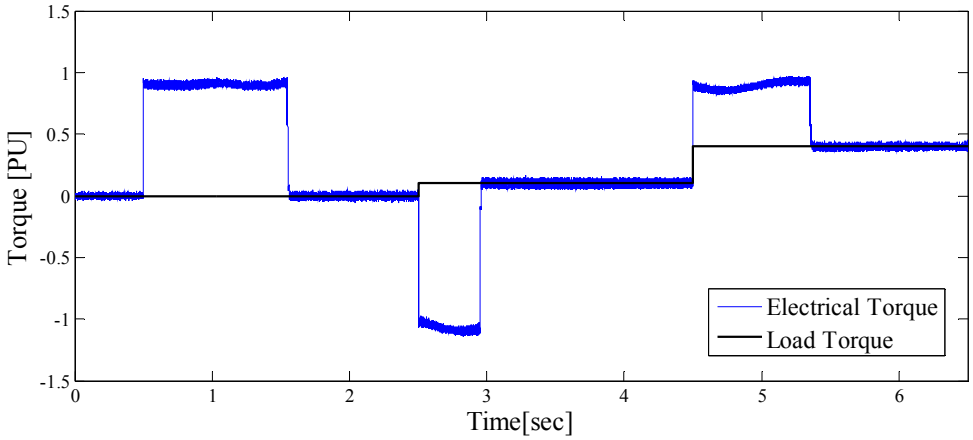

(a)

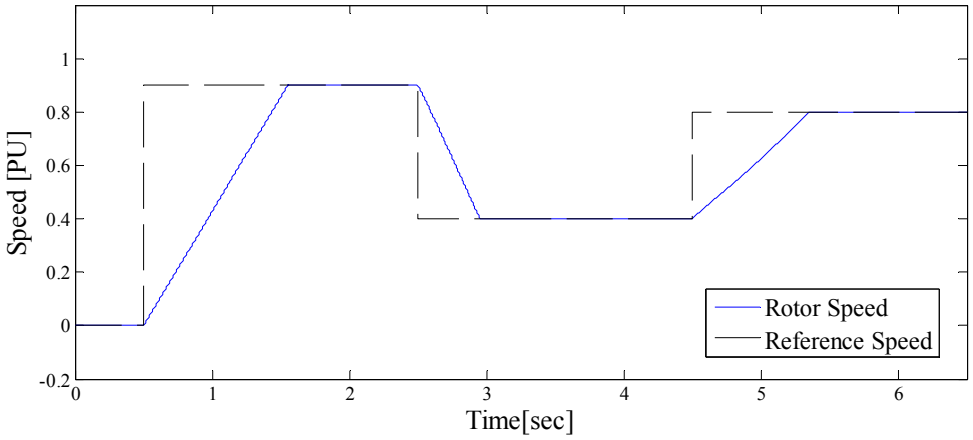

(b)

Figure 4-7 Dynamic response of the induction machine after optimization

(a) Torque Variations (b) Rotor Speed

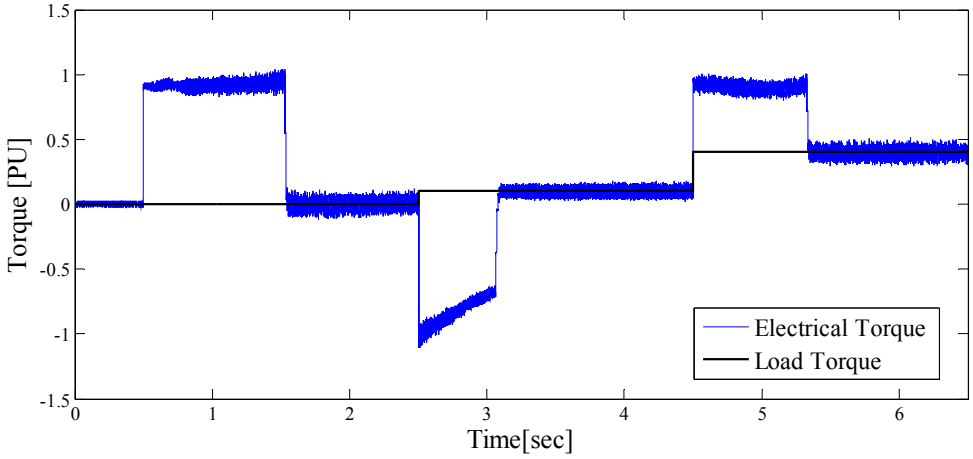

(a)

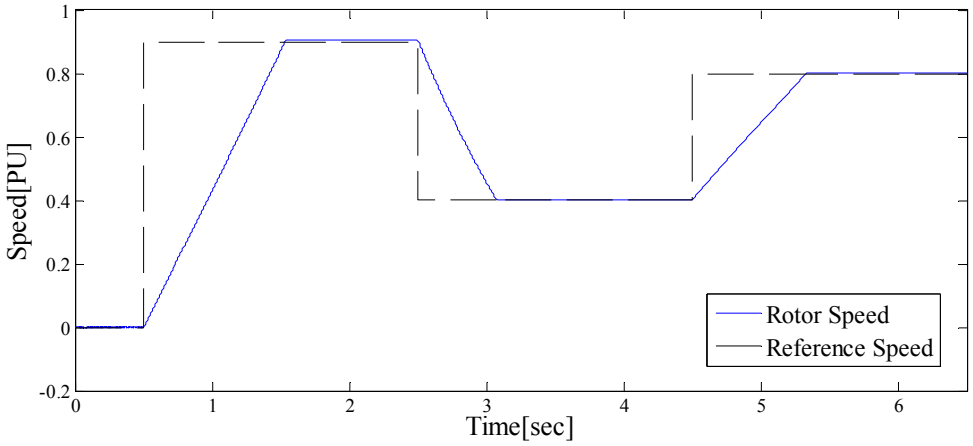

(b)

Figure 4-8 Dynamic response of the induction machine before optimization

(a) Torque variations (b) Rotor Speed

Figure 4-9 illustrates the impact of the optimization on the improvement of the dc link voltage quality.

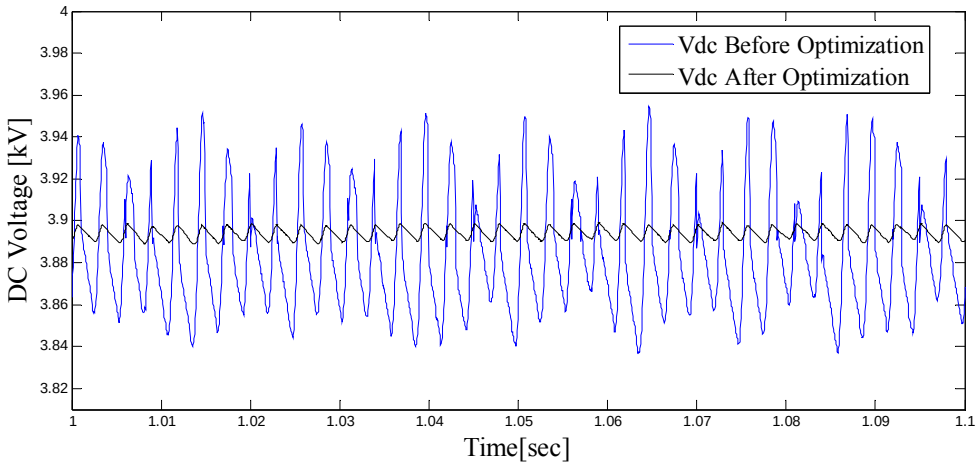

Figure 4-9 dc link Voltage

The simulation results show the great performance of this control methodology during both transients and steady state. Moreover, it was observed that simulation-based optimal design is a useful method to optimize the cost of power elements while improving the performance of the system. Although this control methodology meets the criteria, its sensitivity to machine parameter variations is not desirable. In the next chapter another class of dynamics-based control techniques that overcome this problem is introduced.

Chapter 5

Direct Torque Control Induction Motor Drives

The underlying idea of direct torque control (DTC) of an induction motor is to control both the stator flux and the electromagnetic torque of the machine directly and simultaneously. In this method the stator currents and voltages are controlled indirectly. Both torque and flux of a DTC-based drive are controlled by means of a closed-loop system without using current loops. Moreover, in direct torque control based drives, the concept of the coordinate transformation between stationary reference frame and synchronous reference frame is eliminated in comparison with the vector-controlled drives [34]-[41].

To implement DTC based drives, the stator flux vector and electric torque of the machine need to be estimated precisely. The only machine parameter that is required for stator flux estimation is stator resistance; torque equation does not involve machine parameters for its calculation. Consequently, the sensitivity to parameter variation is significantly reduced in this method [32], [42].

Three methodologies have been employed for implementing DTC drives: (1) the switching table (ST), which is also known as the conventional DTC, (2) the direct self

control (DSC), and (3) the constant switching frequency schemes. ST and DSC regulators are of the hysteresis type [34]-[36], whereas in constant switching schemes digitally implemented analog controllers such as PI controllers are used [42].

In conventional DTC drives the inverter switching states are chosen through a switching table. Since neither current controller nor pulse-width modulation (PWM) modulator is required in this method fast torque response can be achieved. Despite the excellent torque dynamics, this approach is accompanied by some disadvantages [34]-[37].

The main issue is that the inverter switching frequency is not constant for this hysteresis-based DTC scheme. In digital implementation of hysteresis controllers, high sampling frequency for the calculation of torque and flux is required in order to provide good tracking performance and limit the errors of torque and flux within the specified bands, respectively. The inverter switching frequency, which varies with speed of drives and the related error bands, is low in comparison with the system sampling frequency. Furthermore, during starting and low-speed operation the conventional DTC scheme repeatedly selects the zero voltage vectors resulting in flux level reduction owing to the stator resistance drop that results in an undesirable performance.

All the above difficulties can be eliminated when, instead of switching table, a voltage pulse-width modulator is used. Mainly, the constant switching frequencies DTC schemes can be implemented by means of closed loop systems with PI, predictive/dead-beat or neuro-fuzzy controllers [42]. The controllers calculate the required stator voltage vector, averaged over a sampling period. The voltage is finally synthesized by a PWM technique.

In this chapter, it is intended to present the implementation of the DTC scheme operating at the constant switching frequency for an induction motor.

5.1 Principles of DTC

As it was discussed in field oriented control schemes, the electromagnetic torque in a three phase induction machine is controlled by the q-axis stator current, in the synchronous reference frame, as expressed in (1.5):

$$T_e = \frac{3}{2}\frac{P}{2}\frac{L_M}{L_{rr}}\lambda_r i_{qs} = \frac{3}{2}\frac{P}{2}\frac{L_M}{L_{rr}}\lambda_r i_s \sin\delta \qquad (5.1)$$

where P is the number of the poles and δ is the torque angle shown in Figure 5-1, where $\bar{\lambda}_r$ and $\bar{i}_s$ are the rotor flux and stator current respectively, fixed to the stationary reference frame [39] [42].

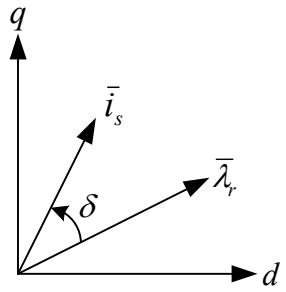

Figure 5-1 Rotor flux and stator current vectors

In the case of voltage source PWM inverter fed induction machine drives, however, not only the stator current but also the stator flux may be used as torque control quantity. In other words (5.1) can be modified to

$$T_e = \frac{3}{2}\frac{P}{2}\frac{L_M}{L_{rr}L_{ss} - L_M^2}\lambda_r \lambda_s \sin(\delta_\lambda) \tag{5.2}$$

δ_λ is the torque angle shown in Figure 5-3. Form the point of view of torque production it is the relative motion of the two vectors that is important, for they form the torque angle δ_λ that determines the instantaneous motor torque. Suppose that the rotor flux moves slowly in counter clockwise direction. Provided that the stator flux magnitude is kept constant, then the electromagnetic torque control can adjusted by changing the angle δ_λ. The way to impose and maintain the required stator flux is via choosing the most suitable voltage source inverter state. For a two-level VSI, the inverter output voltage constitutes six active voltage vectors and two different kinds of zero voltage vectors as shown in Figure 5-2 .

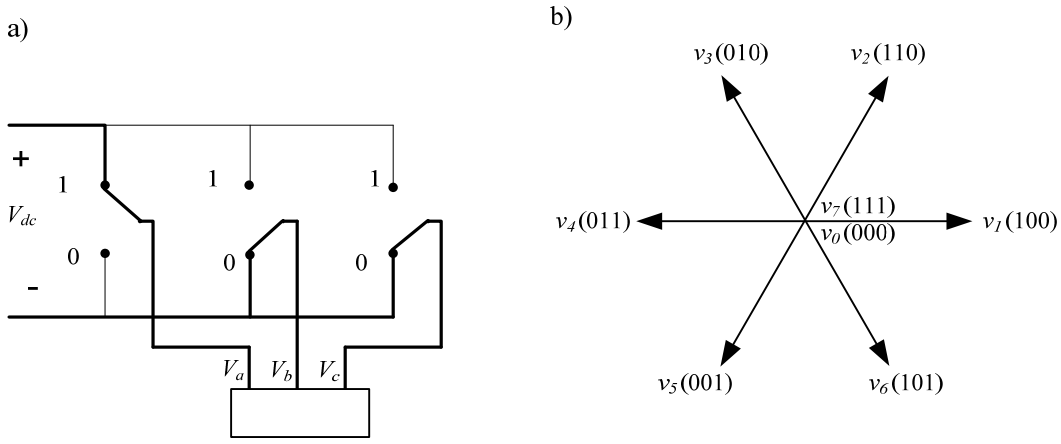

Figure 5-2 a) Simplified diagram of two-level VSI, b) representation of output voltage vectors.

As shown in Figure 5-3, assume that the rotor flux λ_r moves slowly in the counter-clockwise direction. In this case, forward switching of the active voltage vector causes a

rapid movement of λ_s away from λ_r and, therefore the motor torque increases because of the increased torque angle δ_λ [38], [42].

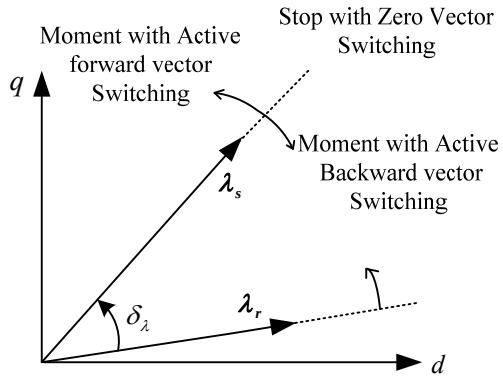

Figure 5-3 Stator flux vector movement relative to rotor flux vector under the influence of active and zero voltage vectors

A significant step to implement high performance DTC-based drives for ac machines is to estimate the stator flux and electric torque properly. To do this the motor model described in the stationary reference frame fixed to the stator can be used.

5.2 Stator Flux Estimation

In the stationary reference frame fixed to the stator, the stator flux is given by

$$\lambda_{sq} = \int \left(v_{sq} - R_s i_{sq}\right) dt$$
$$\lambda_{sd} = \int \left(v_{sd} - R_s i_{sd}\right) dt \tag{5.3}$$

To estimate the motor flux, using an integrator is not suitable due to the following reasons. A pure integrator has drift and saturation problems by initial conditions and the dc offset. The initial value problem related to the pure integrator can change the result significantly. For instance, when the input signal of the integrator is a sine waveform, a cosine wave is expected as its output. But this is true only when the input sine wave is applied at its positive or negative peak. Otherwise, a constant dc offset will appear at the output. This offset, representing a constant dc flux in a motor, does not exist during motor normal operation. The measured motor back emf practically has a dc component that regardless of its value results in the saturation of the pure integrator. Moreover, during the transient operation of the motor when there is rapid change in the integrator input, a dc offset can be generated [43].

To eliminate this problem, a general solution is to employ a first order low pass (LP) filter instead of a pure integrator. Although the filter overcomes the drift and offset problems of the integrator, it produces magnitude and phase angle errors during the motor operation at a frequency lower than the filter cut-off frequency. Therefore, motor drives using LP filters as a flux estimator usually have a limited speed range.

There are several proposed modified integrators to solve the problem of LP filter [43]-[45]. Generally, the transfer function of these integrators can be stated as

$$y = \frac{1}{s+\omega_c} x + \frac{\omega_c}{s+\omega_c} z \tag{5.4}$$

where x is the input signal and z is a compensation signal. The performance of these modified integrators is tightly dependent on the compensation signal. Equation (5.4) implies that if no compensation is assumed for this system, the modified integrator

performs as a first order low-pass filter, which is usually adopted to replace the pure integrator in practice. On the other hand, if the output signal is considered to be the compensation signal ($y = z$) the modified integrator performs the same function as a pure integrator.

Consequently by designing the compensator properly, the modified integrator can be practical for implementation of ac drives operating over a wide range of speed eliminating the problems associated with pure integrator or LP filters. In this research a modified integrator with an adaptive compensation is employed to estimate the flux precisely over a wide range of speed [43]. The performance of this modified integrator along with the adaptive controller is explained in detail as follows. Figure 5-4 illustrates the block diagram of the algorithm.

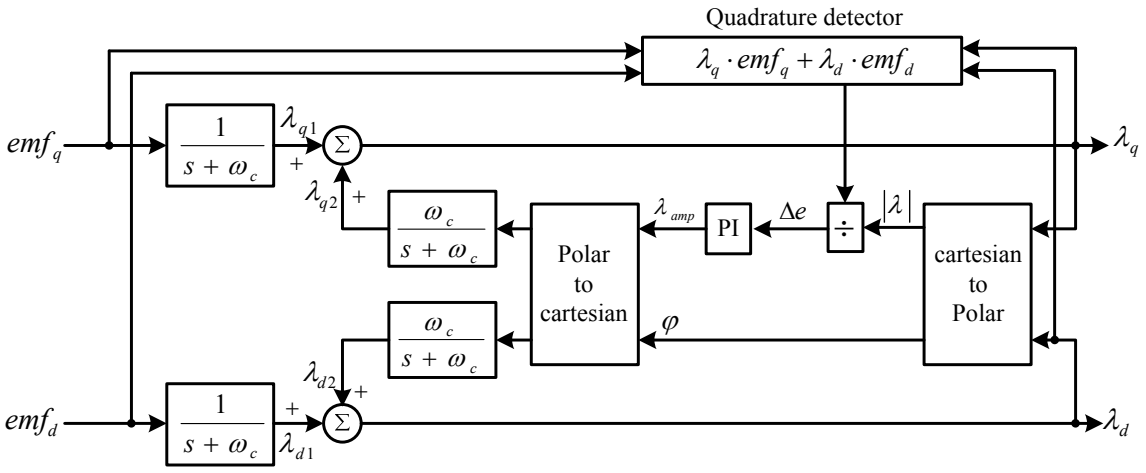

Figure 5-4 Modified integrator with adaptive compensation for flux estimation

In this method the underlying idea is that the motor flux is orthogonal to its back emf. Therefore by means of a quadrature detector the orthogonality between estimated flux

and back emf is detected as explained next. Then by means of a PI controller the appropriate compensation level is generated for the modified integrator to essentially eliminate the initial value and dc drift problems.

The estimated flux λ consists of the feed-forward vector λ_1 (the output of the low-pass filters λ_{q1} and λ_{d1}) and the feedback vector λ_2 (λ_{q2} and λ_{d2}). During normal operation, the flux vector λ should be orthogonal to the back emf vector, thus the output of the quadrature detector is zero. However when an initial value or dc drift is fed into the integrator, the stator flux λ is not orthogonal to the back emf anymore, then an error signal is generated. Figure 5-5 demonstrates this condition.

$$\Delta e = \lambda.emf / |\lambda| = (\lambda_q.emf_q + \lambda_d.emf_d) / |\lambda| = |emf| \cos\gamma \qquad (5.5)$$

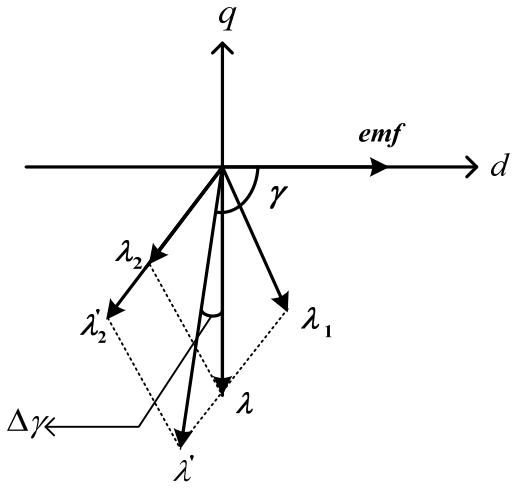

Figure 5-5 Vector diagram showing relationship between flux and emf

In this estimation method, if due to a dc offset or initial condition problem the value of the λ_2 increases to $\lambda_2^{'}$, the angle between the estimated flux $\lambda^{'}$ and back emf is greater than 90^0. Accordingly the quadrature detector will generate a negative error signal, $\Delta e = |emf| \cos\gamma$ which results in reduction of the PI controller output and so the feedback vector. Consequently the estimated flux $\lambda^{'}$ moves to the position of the 90^0 from back emf. Moreover, if the angle γ reduces to less than 90^0 the opposite procedure leads to γ brought back to 90^0.

Now by estimating λ_{ds} and λ_{qs} the magnitude and the position of the stator flux can be obtained by (5.6).

$$\lambda_s = \sqrt{(\lambda_{ds})^2 + (\lambda_{qs})^2}$$
$$\varphi_\lambda = \tan^{-1}\frac{\lambda_{qs}}{\lambda_{ds}} \tag{5.6}$$

5.3 Electrical Torque Estimation

Once the stator flux is estimated properly, the torque can be obtained simply by the machine dynamic equations using stator flux and measured stator current in stationary reference frame fixed to the stator [5]. The electric torque expression that has been obtained in section 2.4 can be used here to calculate the actual torque of the induction machine

$$T_e = \frac{3}{2}\frac{P}{2}\left(\lambda_{ds} i_{qs} - \lambda_{qs} i_{ds}\right) \tag{5.7}$$

where λ_{ds} , λ_{qs} , i_{ds} and i_{qs} are the dq-axis component of the stator flux and current in stationary reference frame fixed to the stator respectively. Figure 5-6 shows the block diagram for torque estimation

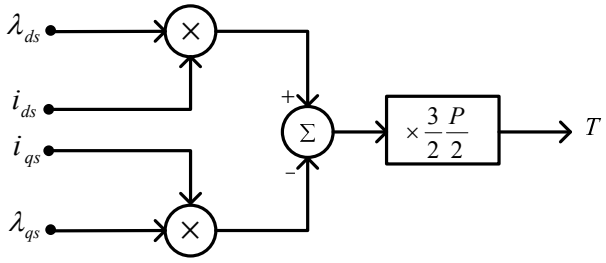

Figure 5-6 Block diagram of torque estimation

5.4 Conventional Direct torque control

The block diagram of the conventional switching table DTC scheme is depicted in Figure 5-7.

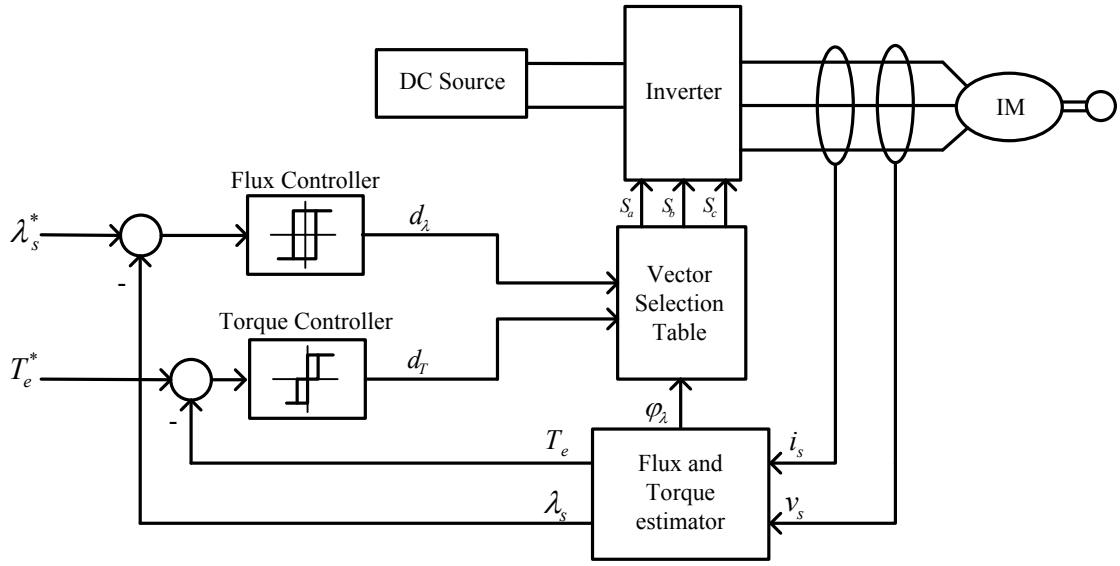

Figure 5-7 Block diagram of the conventional switching table DTC scheme

In this scheme the inverter switching states are determined by torque and flux errors and the position of the stator flux, which is denoted by φ_λ . The torque and flux references are compared with the actual values in hysteresis flux and torque controllers respectively. The flux controller is a two level comparator whereas the torque controller is a three level comparator as will be explained later [38], [42].

As mentioned earlier, there are six active voltage vectors and two different kinds of zero voltage vectors available through a two-level voltage source inverter. Figure 5-8 depicts the possible dynamic zones of the stator flux along with the different possible switching vectors. The possible global zone is divided into six different sectors showed by discontinuous line.

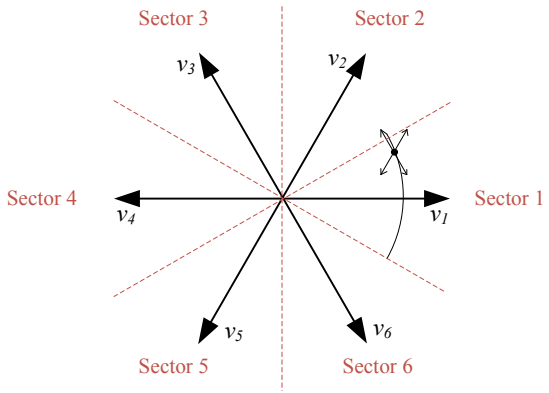

Figure 5-8 Stator flux vector zoness and possible switching voltage vectors

To explain the switching strategy of the conventional DTC, for simplicity the ohmic drops are neglected, then the stator voltage impacts directly the stator flux in accordance with the following equation, driven from (5.3):

$$\frac{d\lambda_s}{dt} = vs \qquad \text{or} \qquad \Delta\lambda_s = v_s \cdot \Delta t \tag{5.8}$$

Decoupled control of the stator flux modulus and torque is achieved by acting on the radial and tangential components respectively of the stator flux linkage space vector in its zone. These two components are directly proportional to the component of the same voltage space vector in the same directions. Figure 5-9 depicts different torque and flux variations depending on the VSI states. In this example the flux vector is assumed to be between $-\pi/6$ and $\pi/6$. States 2 and 3 cause current in quadrature with the stator flux and therefore increase the torque. Similarly, states 5 and 6 cause the torque to decrease. In addition states 2 and 6 cause the flux magnitude to increase and states 3 and 5 decrease the flux magnitude.

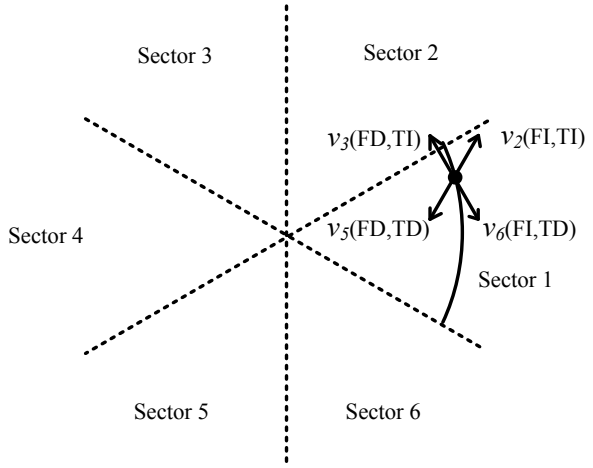

Figure 5-9 Stator flux vector zones, FD: flux decrease, FI: flux increase, TD: torque decrease, TI: torque increace

In accordance with Figure 5-9 the general Table 5-1 can be written. It can be seen from Table 5-1 that the states V_k and V_{k+3} are not considered in the torque because they can both increase (first 30 degree) or decrease (second 30 degree) the torque at the same sector depending on the stator flux position [46].

Table 5-1 General selection table for DTC, *k*: sector number

	Increase	Decrease
Stator Flux	v_k, v_{k+1}, v_{k-1}	$v_{k+2}, v_{k-2}, v_{k+3}$
Torque	v_{k+1}, v_{k+2}	v_{k-1}, v_{k-2}

Now the digitalized variables and the stator flux sector obtained from the angular position, create a digital word that determines the switching commands. The switching commands are listed in Table 5-2 [42], [46], [47].

Table 5-2 Switching table for the conventional DTC of induction motor drives

$d_\lambda d_T$ \ #Sector		Sector 1	Sector 2	Sector 3	Sector 4	Sector 5	Sector 6
$d_\lambda = 1$	$d_T = 1$	v_2	v_3	v_4	v_5	v_6	v_1
	$d_T = 0$	v_0	v_7	v_0	v_7	v_0	v_7
	$d_T = -1$	v_6	v_1	v_2	v_3	v_4	v_5
$d_\lambda = -1$	$d_T = 1$	v_3	v_4	v_5	v_6	v_1	v_2
	$d_T = 0$	v_7	v_0	v_7	v_0	v_7	v_0
	$d_T = -1$	v_5	v_6	v_1	v_2	v_3	v_4

5.5 Constant Switching Frequency DTC-Based Drives

This control scheme relies on a simplified transformation of the stator voltage components in the stator flux oriented coordinates. In this reference frame the q-axis stator flux will be zero then the electric torque is expressed as

$$T_e = \frac{3}{2}\frac{P}{2}\lambda_s i_{sq} \tag{5.9}$$

Therefore, the dq-axis components of the voltage equation can be modified as (5.10) [48]-[50].

$$\begin{aligned} V_{sd} &= R_s i_{sd} + s\lambda_s \approx s\lambda_s \\ V_{sq} &= R_s i_{sq} + \omega_e \lambda_s = K_s T_e + \omega_e \lambda_s \end{aligned} \tag{5.10}$$

where K_s is

$$K_s = \frac{4}{3P\lambda_s} \tag{5.11}$$

As previously stated, the main concept of the direct torque control is to regulate the torque and the magnitude of the flux directly by selecting the proper switching states. The above equations show that the component V_{sd} has influence only on the change of stator flux magnitude; the component V_{sq} can be used for torque adjustment, if the term $\omega_e \lambda_s$ is decoupled. In this scheme, two PI controllers are applied to control both the torque and the magnitude of the flux, by generating the voltage command for inverter control. Therefore the dq-axis components of the reference voltage vector in the mentioned reference frame are

$$\begin{aligned} V_{sd}^* &= \left(K_{P\lambda} + K_{I\lambda}/s\right)\left(\lambda_s^* - \lambda_s\right) \\ V_{sq}^* &= \left(K_{PT} + K_{IT}/s\right)\left(T_e^* - T_e\right) + \lambda_s \omega_e \end{aligned} \tag{5.12}$$

where $K_{P\lambda}$ and $K_{I\lambda}$ are the proportional gain and integration time constant of stator flux and K_{PT} and K_{IT} are the proportional gain and integration time constant of torque

controller. Figure 5-10 shows the block diagram of this control scheme. As it can be seen form (5.12) a decoupling mechanism is required for the q-axis component of the stator voltage [42], [48]-[50].

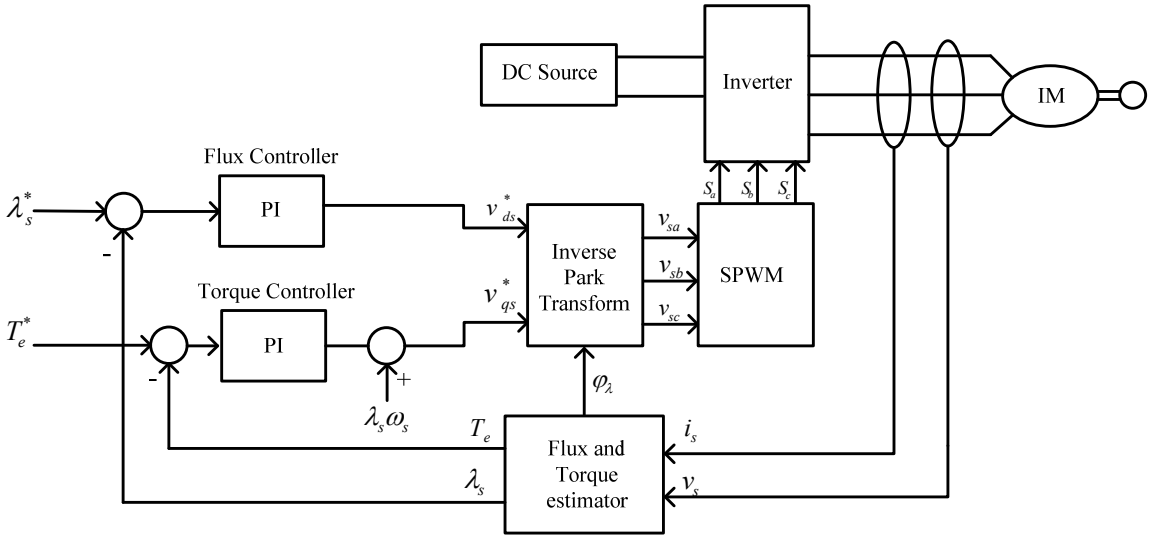

Figure 5-10 Direct Torque Control scheme

5.6 Design Goals and Simulation Based Optimal Result

As mentioned in Chapter 4, the torque and speed of an electric motor are two quantities that should be tightly controlled. On the other hand, designing the *LC* low pass filter for the dc link that provides fast transient response as well as low steady state ripple is another significant step. Therefore to achieve the optimal performance of the DTC-based drive systems, the controller parameters along with the low pass filter elements should be designed properly to fulfill the design objectives. Due to the nonlinear nature of the power electronic devices and complexity of the DTC-based drive systems a computer

simulation model along with an optimization algorithm can be employed to design such systems.

To optimize the performance of the system under transient and steady state conditions, an objective function that is consist of sub-objective functions should be developed to describe the design objectives. Similar to indirect vector control drive case described in section 4.3, the design objectives are

- Minimizing deviation of the actual speed form the set value
- Minimizing the torque ripples
- Minimizing dc voltage ripple
- Cost factor for the size of L and C for the dc link

Therefore (5.13) expresses the objective function designed for this DTC-base drive system.

$$OF_t\left(G_{Vd}, T_{Vd}, G_{Vq}, T_{Vq}, G_{\omega}, T_{\omega}, L_{dc}, C_{dc}\right) = k_1 OF_1 + k_2 OF_2 + k_3 OF_3 + k_1 OF_4 \tag{5.13}$$

where the sub-objective functions are

$$OF_1 = 100 \int_{ss} (\omega_{out} - \omega_{ref})^2 + \frac{1}{100} \int_{transient} (\omega_{out} - \omega_{ref})^2 \tag{5.14}$$

$$OF_2 = \int T^2_{elec-Ripple} \tag{5.15}$$

$$OF_3 = \int V^2_{dc-Ripple} \tag{5.16}$$

$$OF_4 = \frac{C_{dc}[\mu F]}{5000} + 500 L_{dc}[mH] \tag{5.17}$$

(5.14) states that first objective function calculates the deviation of the reference speed from the reference speed during the transient and steady state periods. The second sub-

objective function in (5.15) represents the torque ripples of the machine. The third one, expressed in (5.16), considers the quality of the dc link voltage, whereas the last one (5.17) is to consider the size of the LC low pass filter for the dc link.

As mentioned in Chapter 4, through observing several experiments the weighting factors are obtained based on the range of the variation of the corresponding sub-objective function. These weighting factors are expressed below.

$$K_1 = 200 \quad K_2 = 1500 \quad K_3 = 1500 \quad K_4 = 1 \tag{5.18}$$

5.7 Simulation Case and Optimization Results

To model the constant switching frequency DTC-based drive system the PSCAD/ EMTDC is employed. The detailed model of the power electronic drive along with Direct Torque Control system is illustrated in Figure 5-11. In this DTC-base drive simulation case, the system parameters are selected the same as the vector control drive system listed in Table 4-1.

As it can be seen in Figure 5-11, there are three PI controllers in this drive system to regulate the speed, torque and stator flux linkages of the induction machine. The values of the gain and time constant of these PI controllers are unknown. Moreover the low-pass filter elements in the power circuit are not determined. As explained before, PSCAD/EMTDC has an optimization tool that uses simplex method with the multi-run feature to find the optimum set of parameters that result in the small value of the objective function.

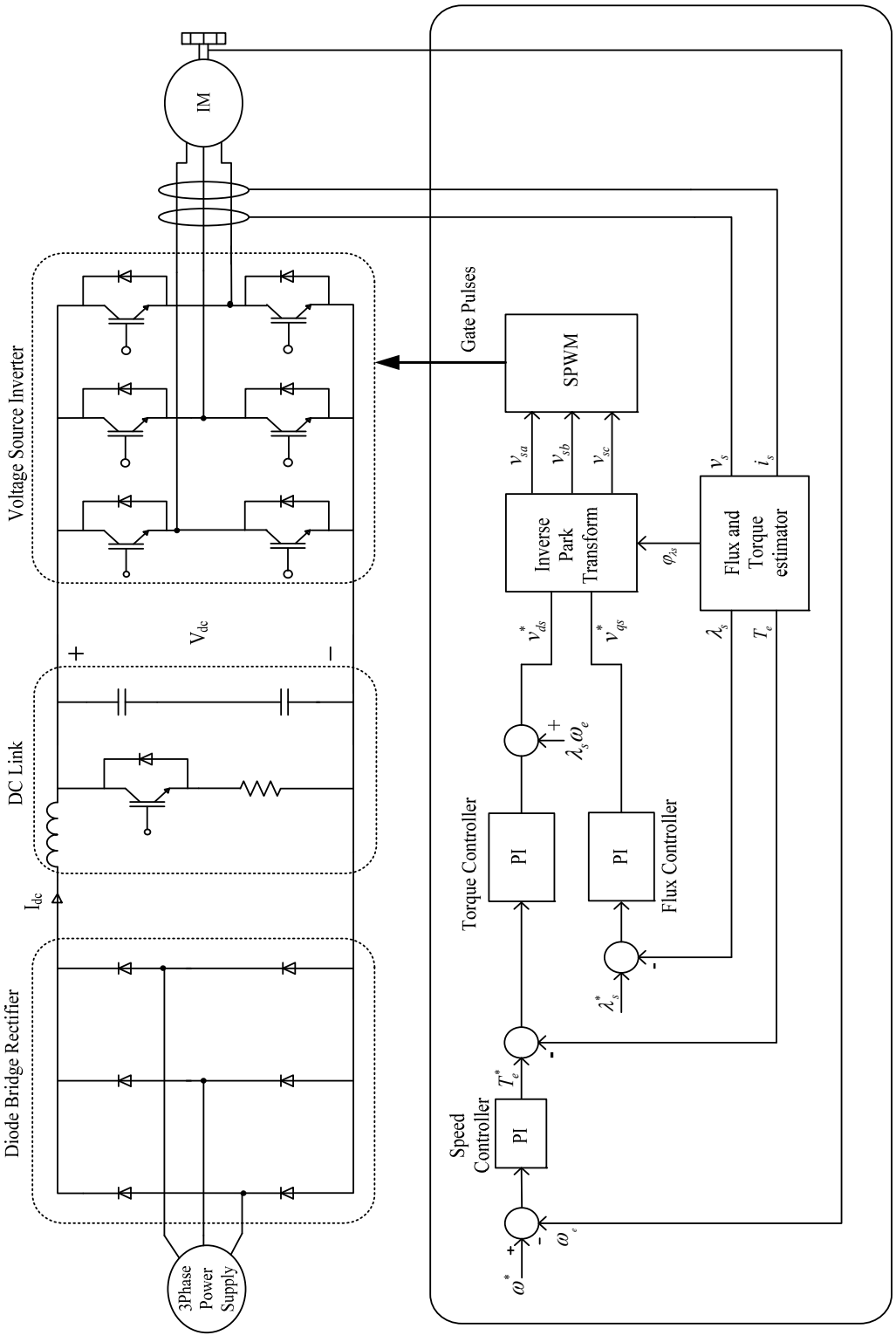

Figure 5-11 Detailed model of the drive system along with the Direct Torque Control controller

In this controller system, the flux should be estimated precisely in a wide range of speed by using the modified integrator with an adaptive compensation. In order to verify the performance of the controller system, the dynamic response of the induction machine should be observed during steady state and transient conditions with various motor loads in wide range of reference speed. Therefore, in this study the motor is operating under the sequence of conditions depicted in Figure 5-12.

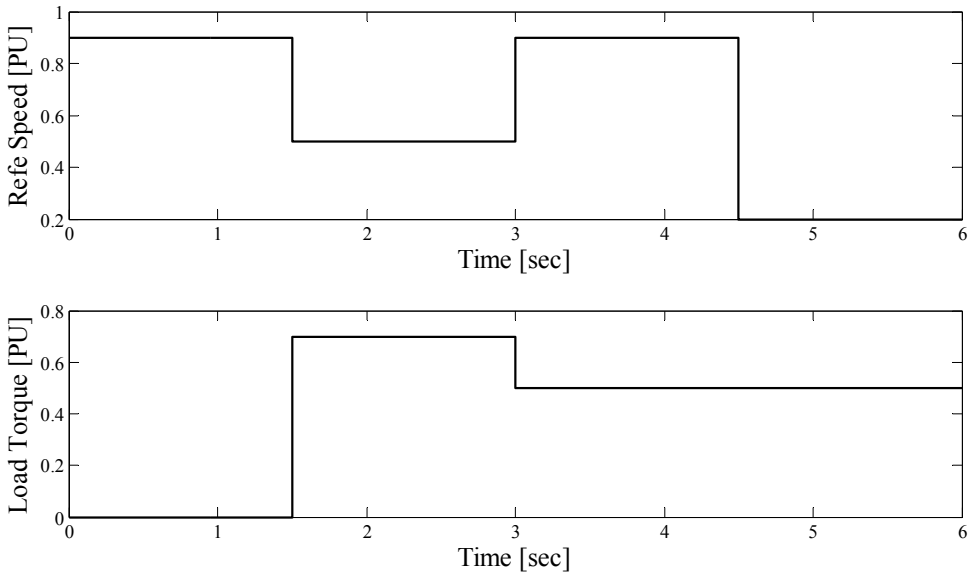

Figure 5-12 Reference speed and load torque variations

To find the optimum point with the minimum value of the objective function, 533 simulations were run (on a 2.67 GHz, dual core machine) and took over 30648.00 seconds (8 hours and 30 minutes). In order to compare the system performance after and before the optimization the objective function values along with the corresponding sub-objective functions are listed in Table 5-3.

Table 5-3 Objective function values before and after optimization

	OF_1	OF_2	OF_3	OF_4	OF_t
Initial	0.0002547	0.012057	0.060976	0.6	148.84
Optimum	0.0000532	0.007573	0.000473	1.5	26.96

Considering sub-objective functions related to torque ripple and speed error before after and before the optimization, it can be observed that the dynamic behaviour of the induction machine is improved significantly. Figure 5-13 and Figure 5-14 show the speed and torque response of the induction machine under different conditions of load torque in a wide range of speed before and after the optimization respectively.

As an initial value for optimization algorithm, the size of the filter elements was chosen to be small, but the optimization showed that by increasing the filter size within an acceptable range, marked improvement in the dc voltage quality is achieved, which leads to minimize the torque ripple. In Figure 5-15, the impact of optimization on improvement of dc voltage can be observed

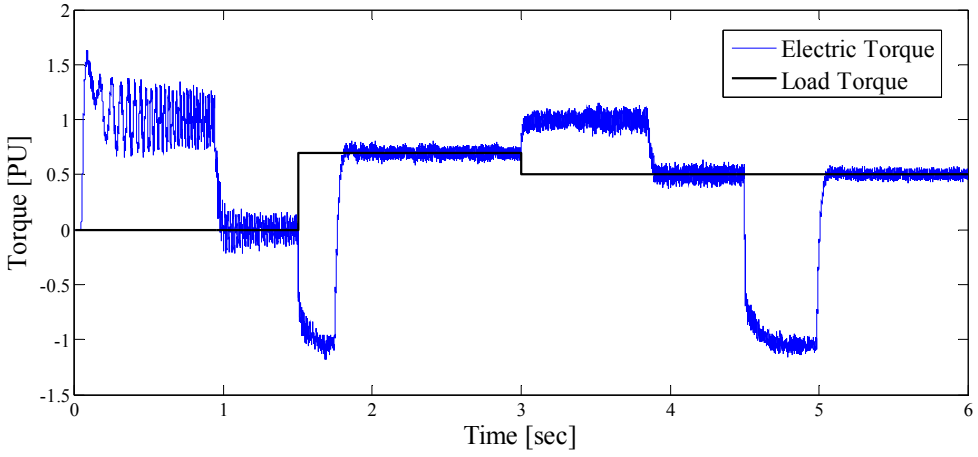

(a)

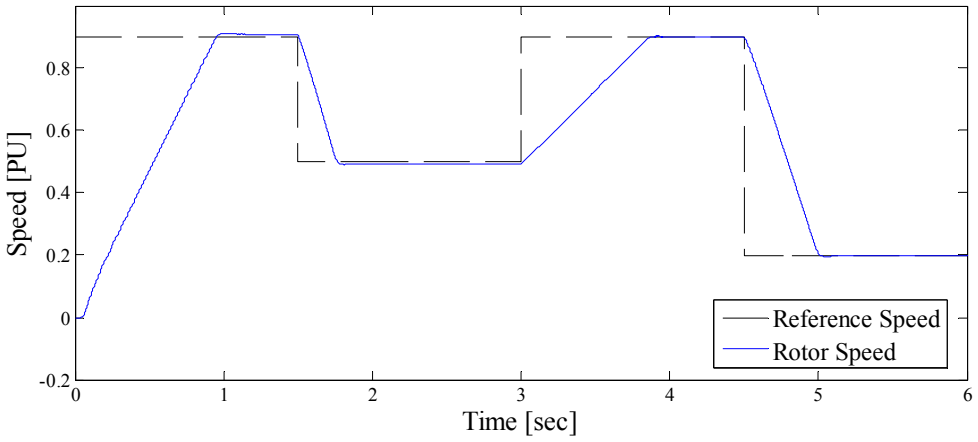

(b)

Figure 5-13 Dynamic response of the induction machine before optimization

(a) Torque Variations (b) Rotor Speed

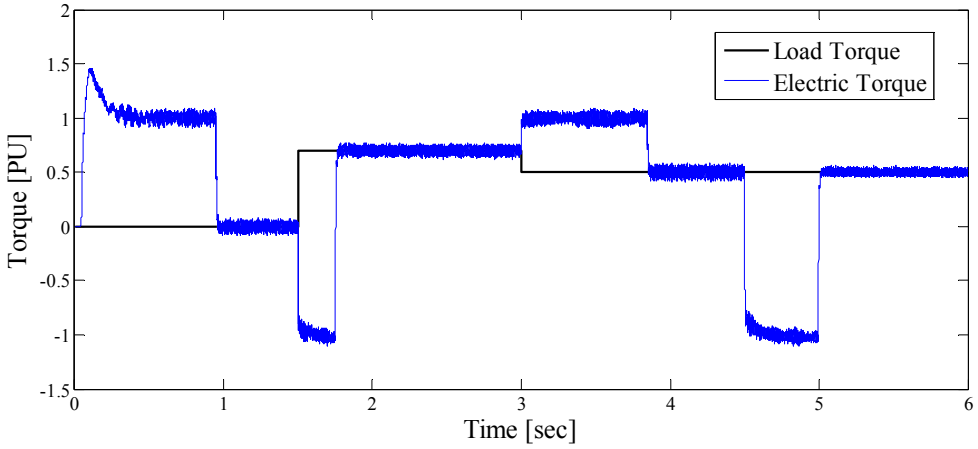

(a)

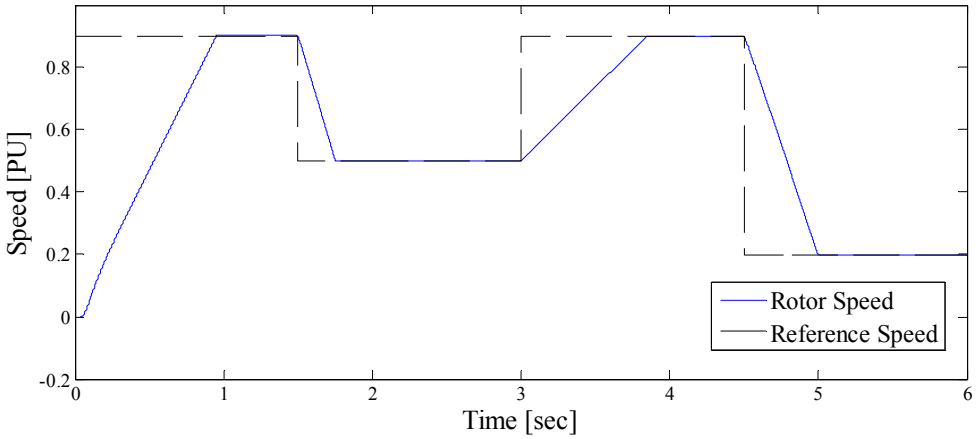

(b)

Figure 5-14 Dynamic response of the induction machine after optimization

(a) Torque Variations (b) Rotor Speed

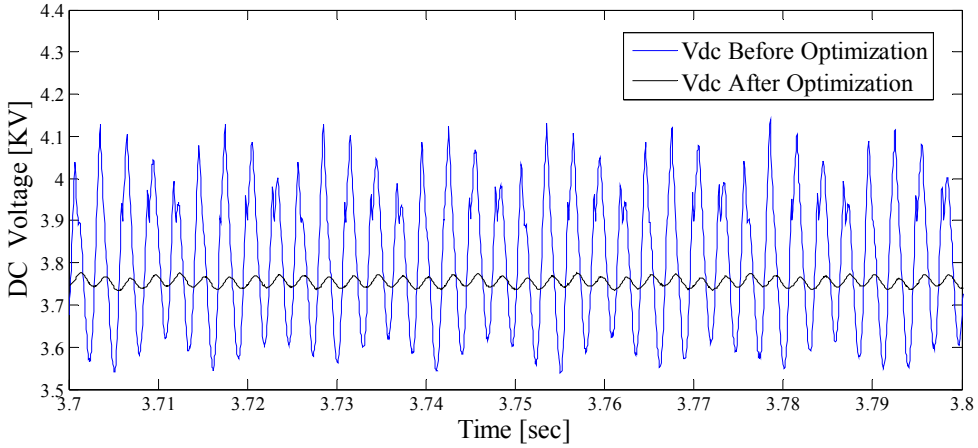

Figure 5-15 dc link Voltage

In this chapter, similar to the indirect vector control drive, the simulation results show the superior performance of the drive system during both transients and steady state. Although the simulation based optimal design requires minimum human interaction to improve the performance of the system, lengthy simulation runs with small time step result in a prolonged design cycle to obtain the optimal set of parameters. Reduced intensity computer models of the fast acting switches of the drive system are possible solutions that will be presented in the next chapter.

Chapter 6

Reduced Intensity Computer Modeling of Power Electronic Inverters

With growing complexity of power electric drive systems and with the extension of using fast acting power electronic controllers in power systems, employing a computer simulation model to design and verify such systems is inevitable. PSCAD/EMTDC is a powerful transient simulator that enables users to implement detailed models of power electronic components and modules (where the switching of all power electronic switches is taken into account).

However using the detailed switching models usually requires extensive computing process, and subsequently an excessive amount of time is consumed. This is because the simulation time step for power switching devices must be chosen to be small (typically in microseconds, and the transient of the system often last for hundreds of milliseconds. Furthermore, the switching action of power electronic devices causes the system to be

discontinuous and nonlinear, which prohibits applying classical control methods for system design and analysis.

A major difference between the simulation of the transient performance of a drive system and that of a typical power system is that a drive system exhibits longer transients due to its mechanical subsystems that have larger time constants. On the other hand, the VSI is operating with a high switching frequency that requires a small simulation time step to achieve reasonable results. Note that the simulation-based optimal design procedure is a repetitive process involving a large number of time-consuming simulations. With a more intensive and longer simulation, it is expected that the simulation-based design of a drive system be massively time consuming and require extensive computing resources. It is therefore imperative to develop methods to expedite the design process.

Marked improvements in simulation intensity are obtained by developing computationally simplified models of the high frequency power electronic converters used in a drive system. In this chapter, equivalent circuits will be developed to remove the time-consuming switching events in the converter simulation while retaining simulation accuracy. Models based on controlled voltage and current sources are shown to be suitable solutions. In this section two sets of models are presented. One is based on the mathematical model of the power electronic system without using the switches, and the other is a dynamic average model.

6.1 Dynamic Average Model of a VSI

Dynamic average modeling of the high frequency power electronic converters is a practical method for reducing their simulation intensity and leads to decreasing the simulation time. In system-level studies, the exact behaviour of the power switching devices is not always a concern, which allows the possibility of using the average model for many simulation cases [51], [52].

Most power electronic converters are linear time-invariant (LTI) circuits for every switching configuration. Averaging different circuit topologies within one switching period T can be applied to remove the high frequency switching events of the circuit. Therefore it can be considered as the first step to eliminate higher order harmonics in the waveforms. The average model replaces the discontinuous switching cells with a continuous system, which forms the basis for developing a small-signal model. Furthermore, the time step used in simulation of average model is significantly less than the appropriate time step for simulation of the switching model, because there is no switching action any longer [51].

Detailed analysis of the switching cells and accurate averaging of the converter waveforms are required to obtain the average value model of the system.

6.1.1 Average model of a two-level voltage source inverter

The detailed model of a two level three phase inverter with power electronic switches is shown in Figure 6-1.

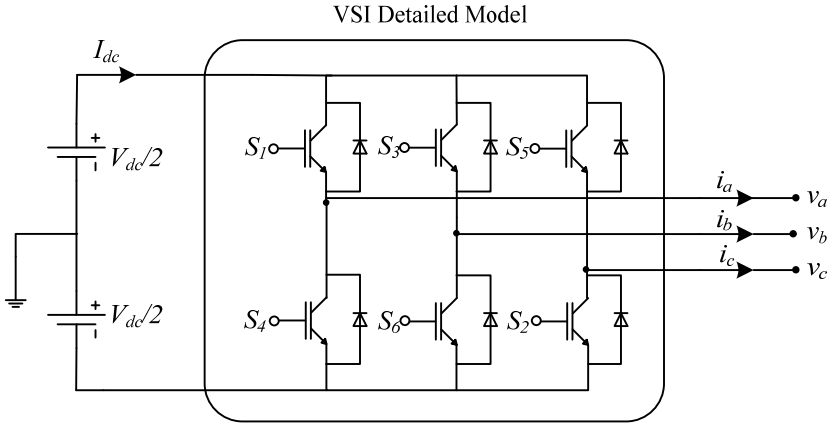

Figure 6-1 Two-level three-phase inverter switching cells

The switching states of the VSI are generated by the SPWM technique. As explained in Chapter 3, in this method the waveform generation is based on comparison of a fundamental frequency sinusoidal reference with a high-frequency triangular carrier waveform. Figure 6-2 represents the triangular wave, the phase-a reference waveform, and the resulting line-to-ground voltage of phase-a. In this figure, the reference waveform of phase-a is shown as a constant value, even if it is in fact sinusoidal. This is because the triangle waveform is considered to be of a much higher switching frequency than the reference waveform. As such the slowly-varying sine wave may be approximated with a constant amplitude within the short period of the carrier waveform.

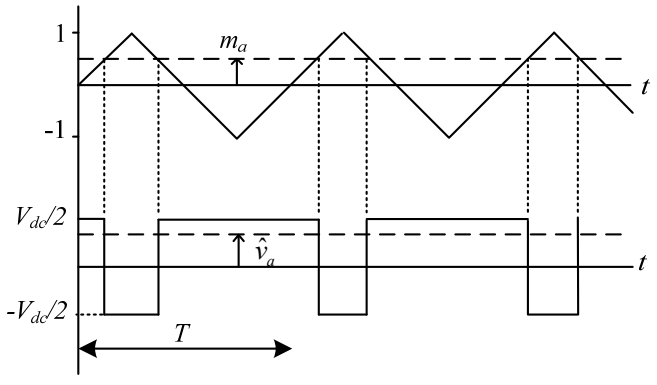

Figure 6-2 Operation of the SPWM Scheme

For the purpose of system analysis, the dynamic average value over the switching period can be used instead of the instantaneous value of the current and voltage. This average function is sometimes referred to as the moving average or fast average. Assuming that T is the switching period, this function can be written as [18]

$$\bar{x} = \frac{1}{T}\int_{t-T}^{t} x(t)\cdot dt \tag{6.1}$$

where $x(t)$ is the state variable that can be voltage $v(t)$ or current $i(t)$. Form Figure 6-2 and (6.1) the dynamic average function of the phase-a output voltages ($\bar{v}_{an}$) can be driven as follows.

$$\bar{v}_{an} = \frac{V_{dc}}{2} m_a \tag{6.2}$$

Similarly it can be shown that,

$$\bar{v}_{bn} = \frac{V_{dc}}{2} m_b \tag{6.3}$$

$$\bar{v}_{cn} = \frac{V_{dc}}{2} m_c \tag{6.4}$$

where $\bar{v}_{an}$ and $\bar{v}_{an}$ are the average value of the phase-b and phase-c voltages, respectively. m_a, m_b and m_c are the sinusoidal reference waveforms that have the same magnitude with 120º phase shift to generate symmetrical three phase output.

$$\begin{aligned} m_a &= m\cos(\theta_c) \\ m_b &= m\cos(\theta_c - 2\pi/3) \\ m_c &= m\cos(\theta_c + 2\pi/3) \end{aligned} \tag{6.5}$$

In the above equations θ_c is the converter voltage angle and m is the modulation index. The output phase voltages can be obtained by substituting the reference waveform equations into the voltage equations as follows [18].

$$\begin{aligned} \bar{v}_a &= \frac{V_{dc}m}{2}\cos(\theta_c) \\ \bar{v}_b &= \frac{V_{dc}m}{2}\cos\left(\theta_c - \frac{2\pi}{3}\right) \\ \bar{v}_c &= \frac{V_{dc}m}{2}\cos\left(\theta_c + \frac{2\pi}{3}\right) \end{aligned} \tag{6.6}$$

Due to high efficiency of the power electric converters in many applications, the conduction losses can be neglected in analysis of the transient behavior of the power electric converters. By applying the energy conversion principle to the converter cell (assuming an ideal converter) the power on the dc link is equal to the ac side power [51].

$$\begin{aligned} P_{dc} &= P_{ac} \\ V_{dc}\cdot I_{dc} &= \frac{3}{2}\left\|\bar{v}_{dq}\right\|\left\|\bar{i}_{dq}\right\|\cos(\phi) \end{aligned} \tag{6.7}$$

In (6.7) ϕ is the power factor angle, and $\bar{v}_{dq}$ and $\bar{i}_{dq}$ are the dq-axis components of the stator voltage and current in arbitrary reference frame, respectively. In this case the reference frame in which the d-axis component of the voltage is equal to zero is chosen to simplify the analysis. Therefore the dq-axis components of the phase voltages in this reference frame are as follows.

$$\bar{v}_q = \frac{V_{dc} m}{2}$$
$$\bar{v}_d = 0 \tag{6.8}$$

Substituting (6.8) in (6.7), the dc link current can be expressed as follows.

$$I_{dc} = \frac{3}{4} m \left\| \bar{i}_{dq} \right\| \cos(\phi) \tag{6.9}$$

The resulting dynamic average model of the VSI is shown in Figure 6-3.

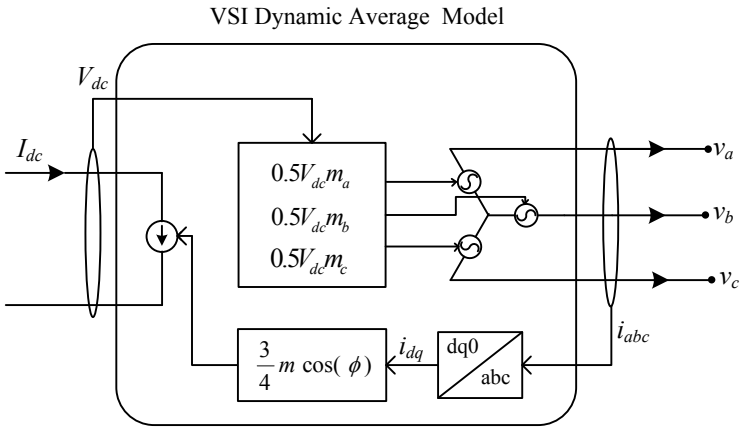

Figure 6-3 Average-value model for the voltage source inverter with SPWM

6.1.2 Average Model Examples

In Chapters 4 and 5 two drive cases were modeled in detail considering the switching of all power electronic switches. To validate the accuracy and to demonstrate the benefits of the VSI dynamic average model in power electronic drive applications, these examples are considered to be examined with average model.

In these drive systems the voltage source inverter is a part of the power electronic system that connects the dc link to the induction machine. The switching frequency of this converter is 10 kHz and the circuit topology changes within every switching period.

Therefore it requires that the simulation time step be chosen small (approximately 10 μs for detail model of the example cases) to obtain accurate simulation results. Since there is no longer any switching event in the average model, accurate result (from an average standpoint) can be obtained even with much larger time steps. Tables and graphs in this section demonstrate that the average model can save a significant amount of time for simulation of such systems.

In vector control and DTC drive systems, the dq-axis component of the reference voltage is generated by the associated controller system and it is transformed to phase voltages through inverse park transformation. Then the generated voltages with the proper normalization is fed into a sinusoidal PWM unit as reference voltage to control the three phase VSI.

In average model, the ac side voltage is calculated by equation (6.6) and it is fed into the stator winding by dependent voltage sources. Then the stator phase currents, which are obtained by the machine model, are employed to calculate the dc link current (using (6.9)) and then will be injected to the dc link by a dependent current source. The simulation results for both drive cases are described below.

a) Example 1: Indirect vector control drive system

Figure 6-4 shows the simulation results of the detailed model along with the average model for a simulation time step of 10 μs. To verify the accuracy of the results for larger time steps in the average model, this model is simulated with the time step of 50 μs as well. The simulation results in this case are shown in Figure 6-5. Note that for the average model the simulation time step has to be small enough to accurately model the response of the controller system.

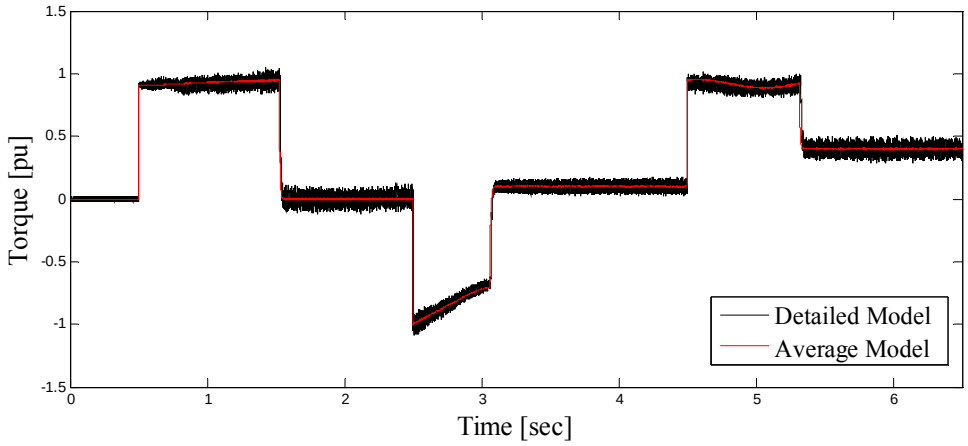

(a)

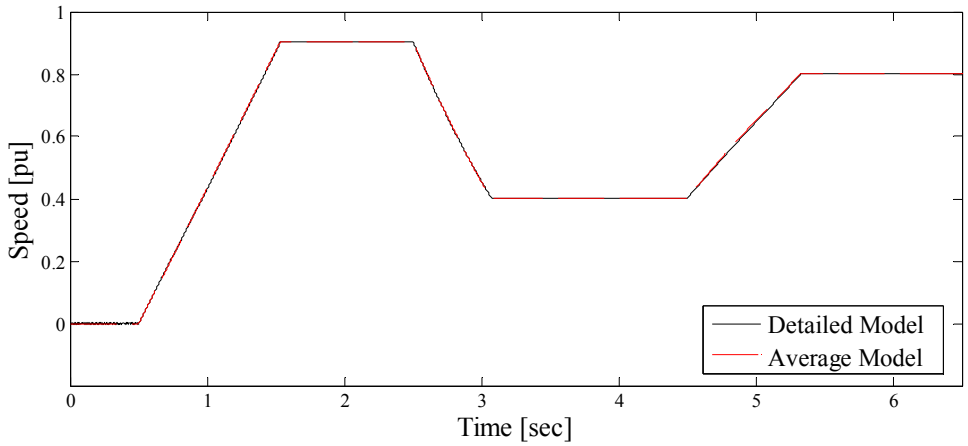

(b)

Figure 6-4 Dynamic response of the vector control drive system for detailed and average model, time step= 10 μs, (a) Torque variations, (b) Rotor speed.

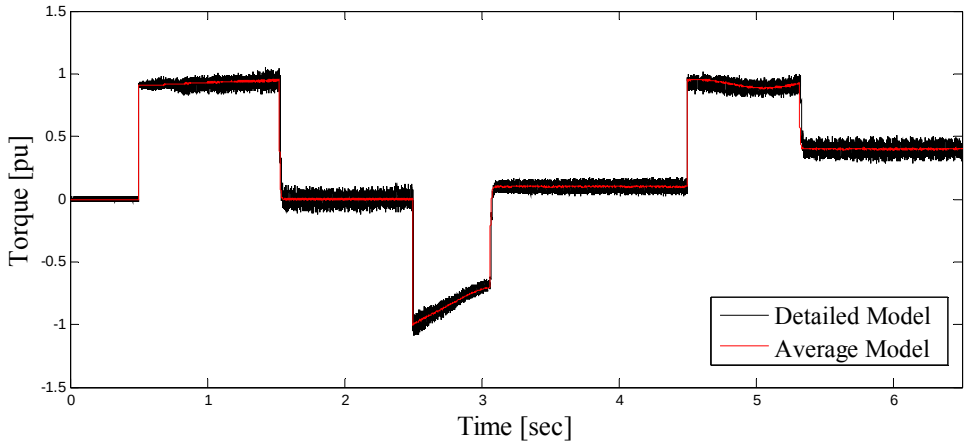

(a)

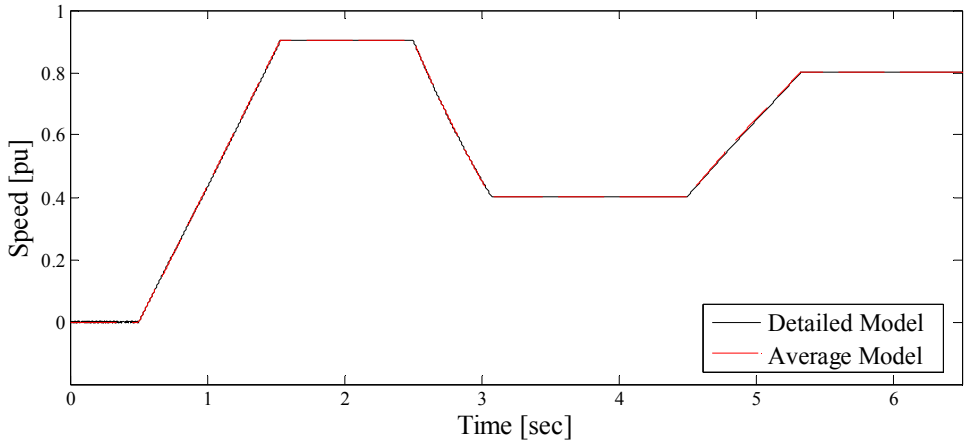

(b)

Figure 6-5 Dynamic response of the vector control drive system for detailed and average model, time step= 50 μs, (a) Torque variations, (b) Rotor speed.

Table 6-1 compares the simulation time of detailed model and average model with different time steps. It can be observed that using the average value model reduces the simulation time by approximately 70 percent when the simulation time step is the same as detailed model. Furthermore, increasing the simulation time step while the accuracy of the average waveforms are maintained results in a significant improvement in simulation time (approximately one tenth).

Table 6-1 Average and detailed model simulation time for vector control drive system

	Time Step	Simulation Time
Detailed Model	10 μs	83.9 s
Average Model	10 μs	23.6 s
	50 μs	7.9 s

b) Example 2: Direct torque control drive system

The second example case to verify the average model is the direct torque control drive system for an induction machine. Similar to vector control drive case, in this example the simulation results of the average model with different time steps are presented.

Figure 6-6 and Figure 6-7 show the torque and speed response of the machine with simulation time step of 10 μs and 50 μs respectively. As shown in these figures, the results of the average model for both simulations are essentially the same.

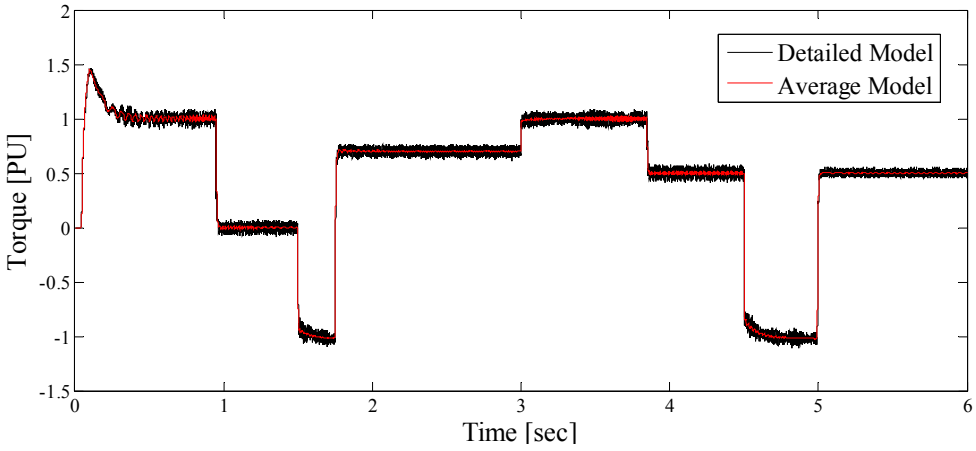

(a)

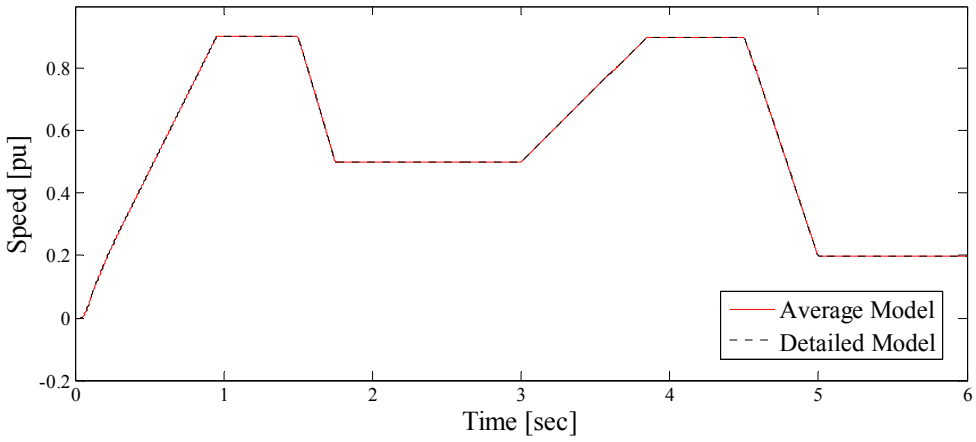

(b)

Figure 6-6 Dynamic response of DTC drive system for detailed and average model, time step= 10 μs, (a) Torque variations, (b) Rotor speed.

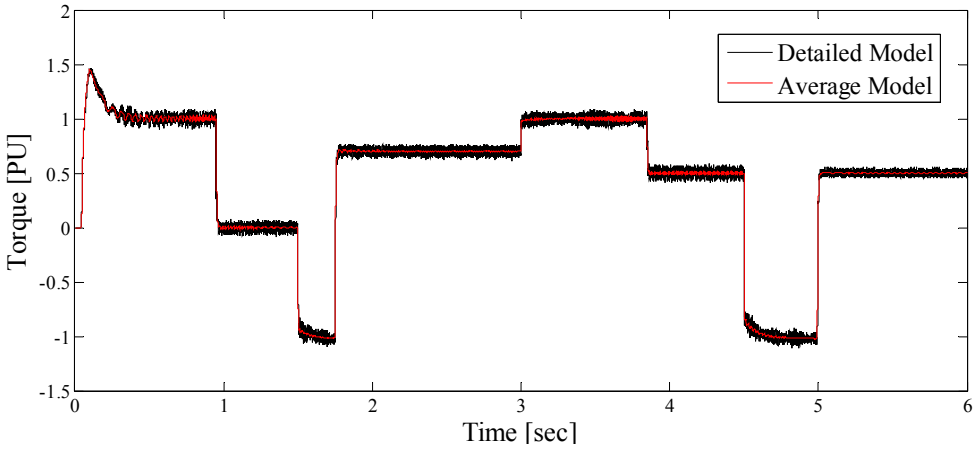

(a)

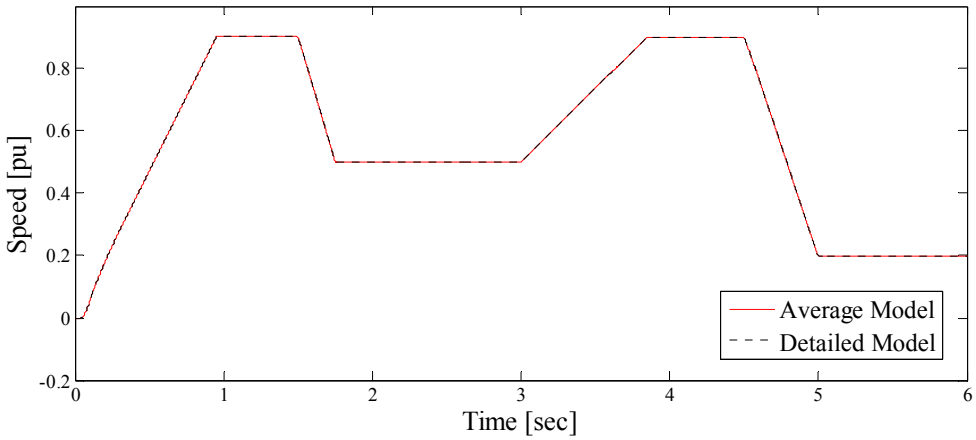

(b)

Figure 6-7 Dynamic response of DTC drive system for detailed and average model, time step= 50 μs, (a) Torque variations, (b) Rotor speed.

The simulation time for average and detailed model are listed in Table 6-2. Similar to example 1, it reveals that the average model offers significant saving in simulation time without loss of accuracy.

Table 6-2 Average and detailed model simulation time for DTC drive system

	Time Step	Simulation Time
Detailed Model	10 μs	58.3 s
Average Model	10 μs	18.9s
	50 μs	6.1 s

6.2 Mathematical Model of a VSI

PSCAD/EMTDC is a nodal analysis based software package [53], [54]. The underlying solution approach is based on discretizing the differential equations for each circuit component using an explicit trapezoidal rule for integration. The network nodal equation has the following general form.

$$GV_n = I_h \tag{6.10}$$

where, G is the network nodal construction matrix, and the vector I_h includes the history current sources and independent sources injected to the nodes. The unknown parameters are nodal voltages V_n that are calculated by solving (6.10) at every time step.

The time step in the EMTDC solution is fixed. Therefore for a specific simulation case, the time step should be chosen small enough so that the network topological changes do not happen inside a time step. At every time step, the network variables are computed to perform the test for the changes in topology. If a change in topology at a

given time step is detected (turning on or off of the power electronic switches) the system is updated for the new topology and is solved again.

As stated earlier, the switching frequency of the VSIs considered in this thesis is 10 kHz and the circuit topology changes within every switching period. Therefore the network nodal construction matrix should be recalculated and inversed at all the switching events. Consequently the simulation of such system requires excessive computations that results in a longer simulation time. Another efficient solution for this problem is to replace the VSI switching circuit with its mathematical model. To develop this model, the VSI is assumed as a block box, and for each operating point, the relationship between the input and output should be calculated.

First the relationship between the output ac voltage and the switching function should be obtained. In two-level voltage source inverters, each output phase voltage is either $0.5V_{dc}$ or $-0.5V_{dc}$, depending on whether the upper or lower switches are conducting. As mentioned in Chapter 3, since the upper and lower switches cannot turn on/off simultaneously, the switching states of the upper and lower switches in each leg are complementary. Therefore the phase voltages can be summarized as follows.

$$v_{an} = \frac{V_{dc}}{2}(s_a - \bar{s}_a) = \frac{V_{dc}}{2}(2s_a - 1)$$

$$v_{bn} = \frac{V_{dc}}{2}(s_b - \bar{s}_b) = \frac{V_{dc}}{2}(2s_b - 1) \qquad (6.11)$$

$$v_{cn} = \frac{V_{dc}}{2}(s_c - \bar{s}_c) = \frac{V_{dc}}{2}(2s_c - 1)$$

where v_{an}, v_{bn} and v_{cn} are the terminal phase a, b and c voltages, and the s_a, s_b and s_c are the upper legs switching states of the related phase respectively. Due to high efficiency of power electronic converters in many power applications, the dc line current can be derived using the principle of conversion of the energy. Assuming an ideal converter, the three phase power is equal to the dc side power.

$$P_{ac}(t) = P_{dc}(t)$$
$$P_{dc}(t) = V_{dc}.I_{dc} \tag{6.12}$$

Therefore the dc link current can be obtained by dividing the instantaneous ac power by the dc voltage. The developed mathematical model is shown in Figure 6-8.

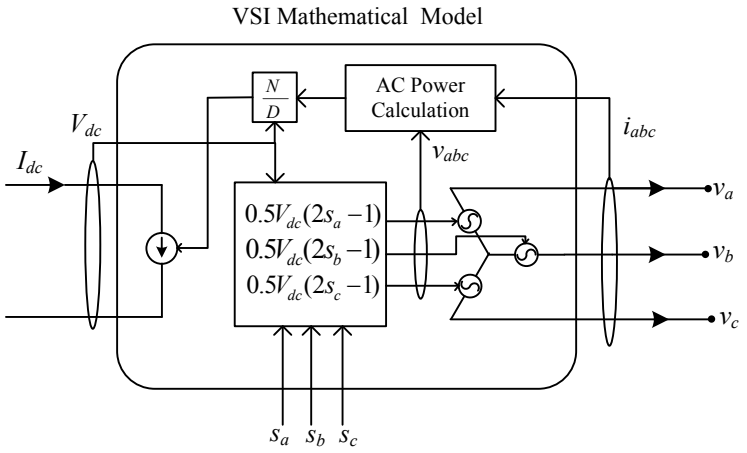

Figure 6-8 Mathematical model of two-level three-phase Voltage Source Inverter

6.2.1 Mathematical Model Examples

Using this VSI model instead of the detailed model in vector control and DTC drive systems demonstrates the reduction in the simulation intensity and accordingly the simulation time. Note that in this case the simulation time step should be the same as the

detailed model, since the switching function with frequency of 10 kHz is used to calculate the terminal voltages and the simulation results is desired to be the same as detailed model. The simulation results for both drive cases are as follows. Since the mathematical model is developed assuming the converter is lossless, the small difference between the simulation results of detailed and mathematical model is expected to be observed.

a) Example 1:Indirect vector control drive system

Figure 6-9 shows the speed and torque of the induction machine with detailed and mathematical model of VSI. To compare the simulation time for detailed and mathematical models Table 6-3 is presented. It can be observed that using the mathematical model results in simulation time saving of approximately 70 percent while the results are the same.

Table 6-3 Mathematical and detailed model simulation time for vector control drive system

	Simulation Time
Detailed Model	83.9 s
Mathematical Model	27.49 s

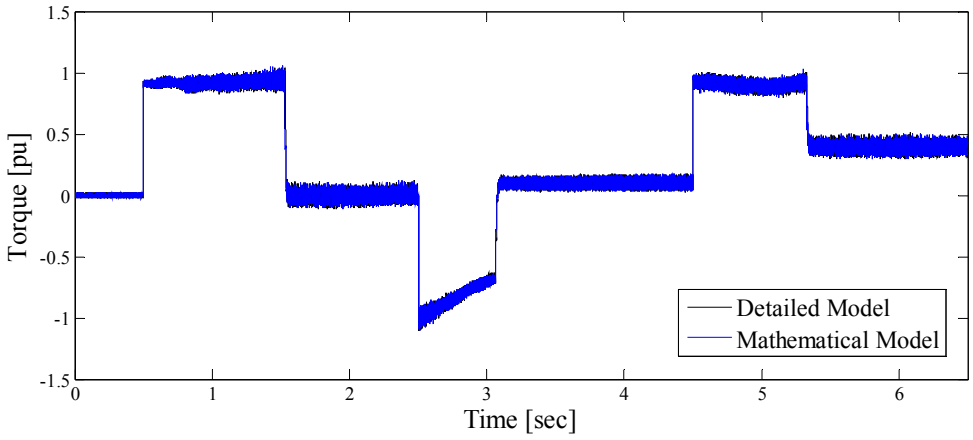

(a)

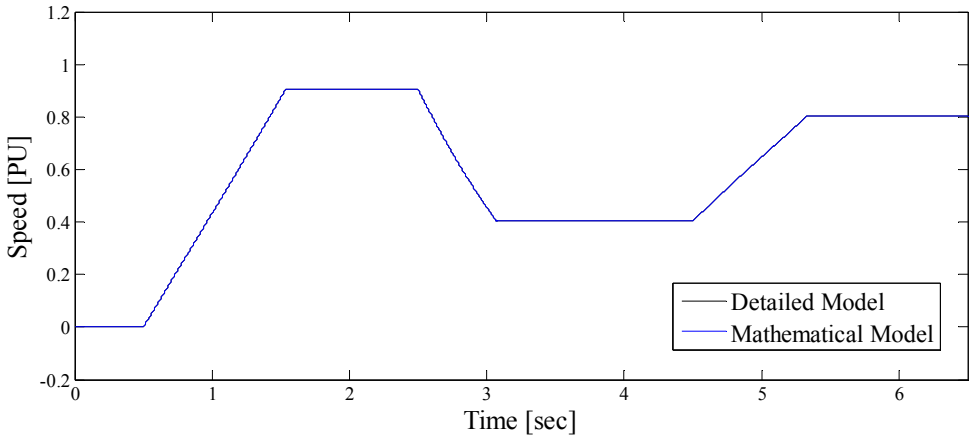

(b)

Figure 6-9 Dynamic response of vector control drive system for detailed and mathematical model, (a) Torque variations, (b) Rotor speed.

To have a more precise observation the simulation results of the torque, ac current and dc voltage in a small time interval are presented in Figure 6-10.

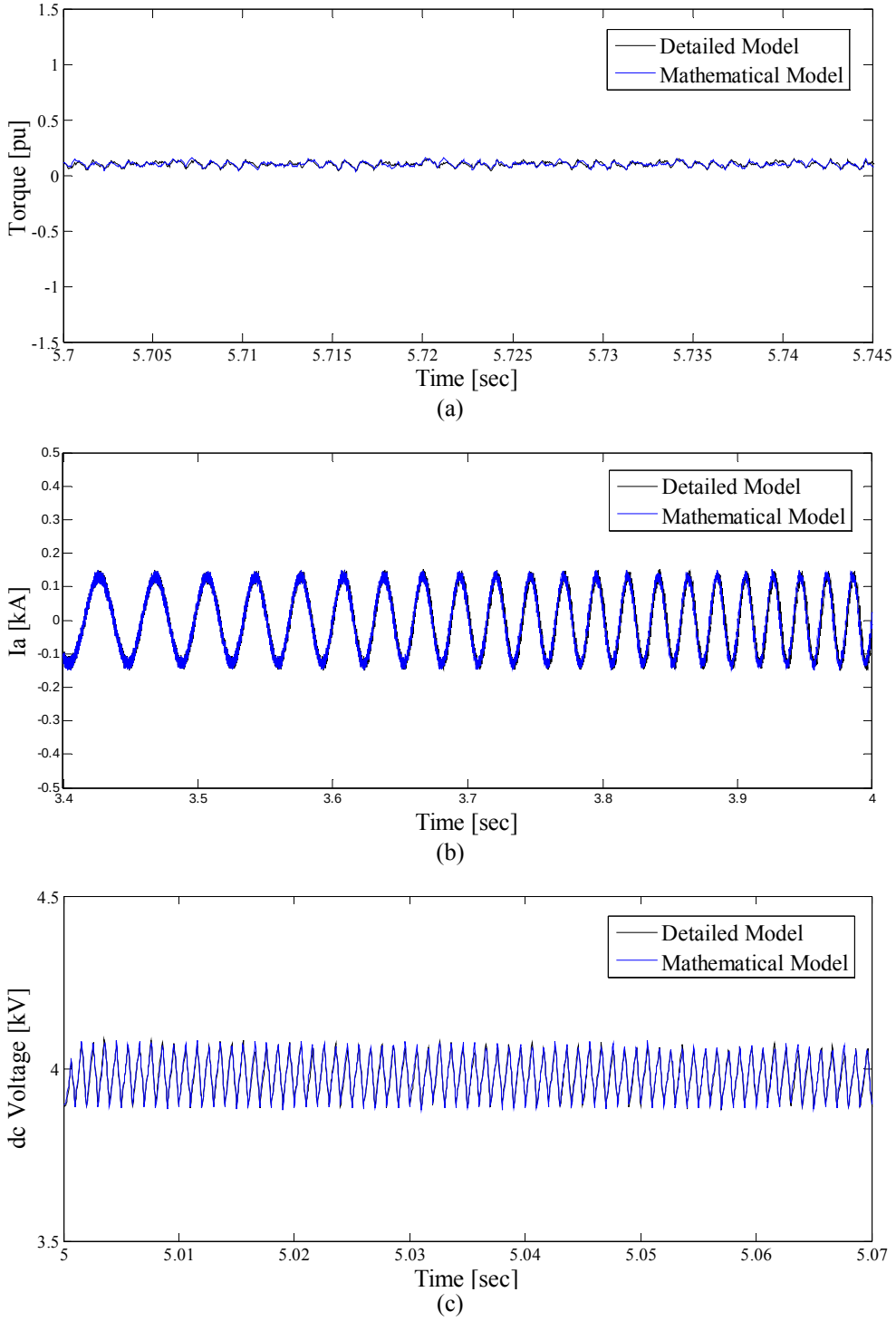

Figure 6-10 Dynamic response of the vector control drive system for detailed and mathematical model, (a) Torque variations, (b) ac current, (c) dc voltage.

b) *Example 2: Direct torque control drive system*

The simulation results of torque and speed of the induction machine for detailed and mathematical model of VSI is shown in Figure 6-11.

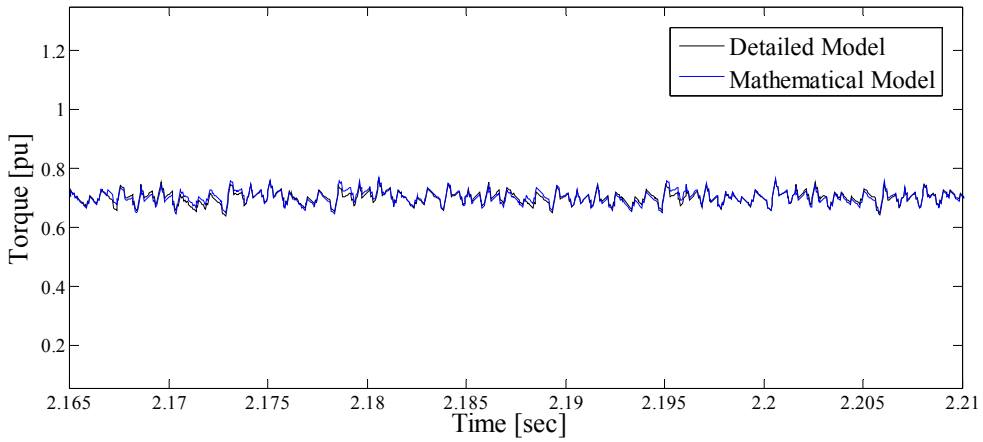

(a)

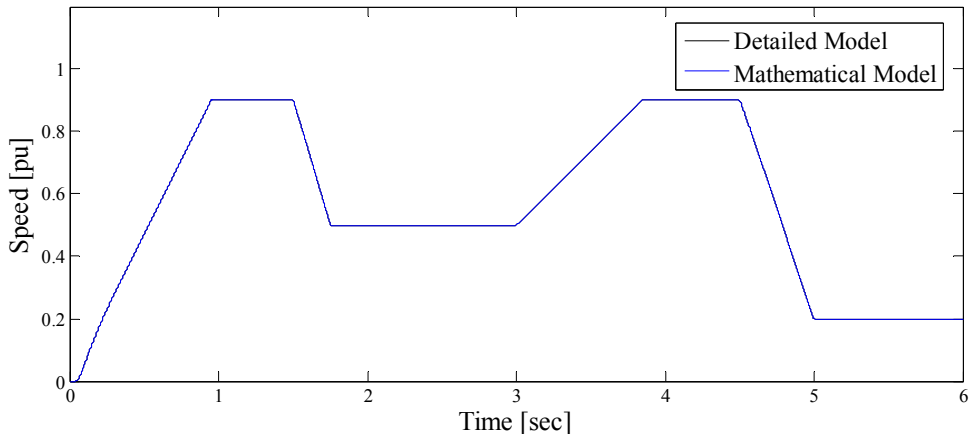

(b)

Figure 6-11 Dynamic response of DTC drive system for detailed and mathematical model

(a)Torque variations (b) Rotor speed

The torque, ac current and dc voltage in a small time interval are shown in Figure 6-12.

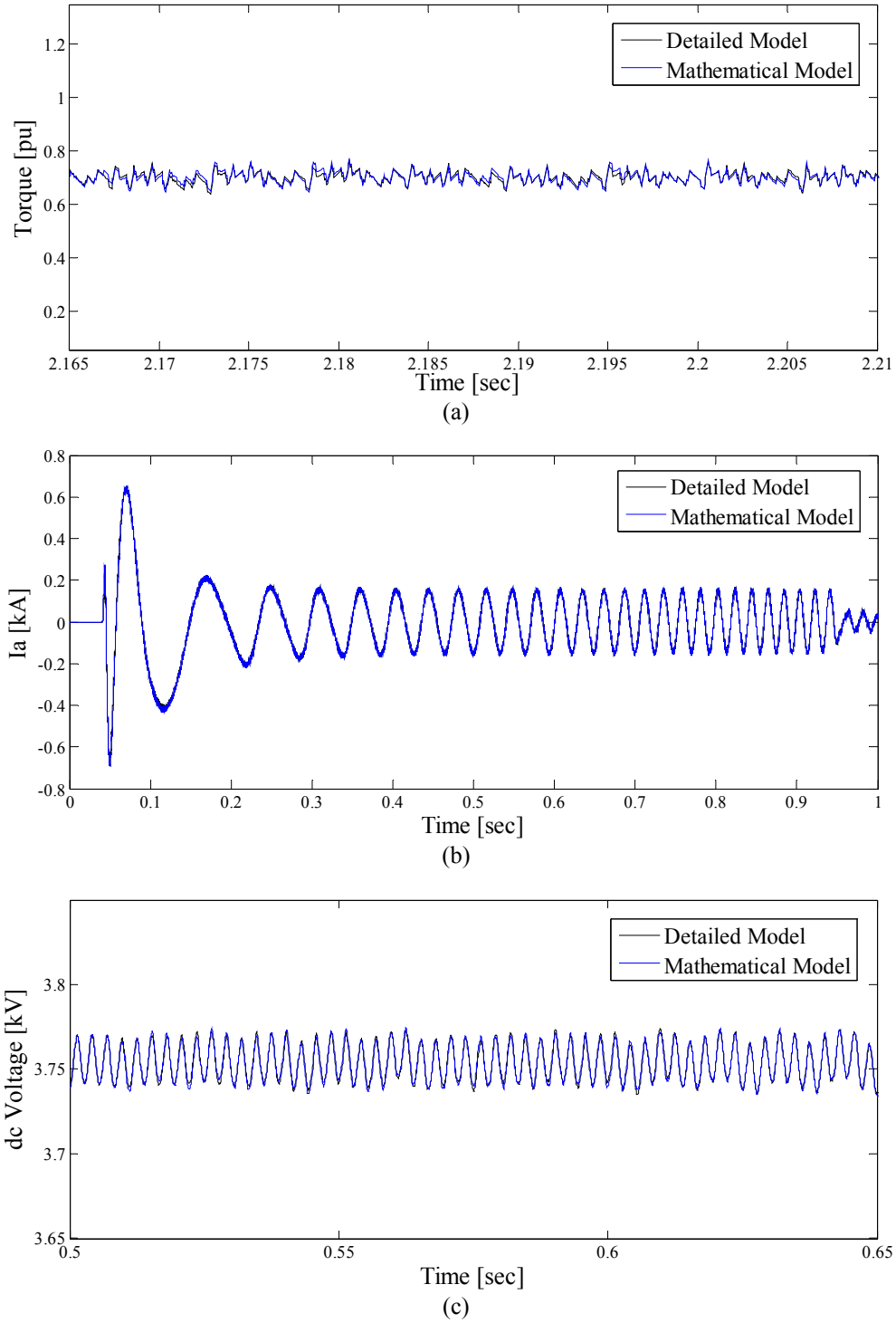

Figure 6-12 Dynamic response of DTC drive system for detailed and mathematical model

(a) Torque variations, (b) ac current, (c) dc voltage.

To compare the simulation time of the detailed and mathematical model Table 6-4 is presented and similar to example 1 the simulation time is reduced by approximately 70 percent.

Table 6-4 Mathematical and detailed model simulation time for DTC drive system

	Simulation Time
Detailed Model	58.3 s
Mathematical Model	19.5 s

In this chapter the procedure for developing reduced intensity computer models including average value model and mathematical model were described. The simulation time tables show that regardless of the control methodologies these models are capable of reducing simulation intensity and time significantly.

Chapter 7

Conclusions and Future Directions

At the first stage of this thesis simulation based optimal designs for two high performance induction machine drive systems based on vector and direct torque control methodologies were developed. Then the average value model and the proposed mathematical model of the power electronic inverters were introduced to reduce the computational intensity of the network in order to reduce the simulation time. The aim of this chapter is to highlight the findings of the thesis and state directions along which this work can be extended.

7.1 Thesis Conclusions and Contributions

The main conclusions and contributions of this research are highlighted as follows:

1. This thesis has reviewed the dynamic and steady state model of induction machine and expressed the time independent equations of the voltage, current, and torque equations in the dq0 reference frame using Park's transformation. Then a highly used ac drive circuit is introduced and three stages in conversion process are explained.

2. The principles of high performance drive control methodologies, vector control and direct torque control, which are based on the dynamic model of machine, are studied thoroughly.
3. Considering the advantages and disadvantages of different categories of each control strategies, simulation based design using PSCAD/EMTDC is done for indirect vector control and constant switching direct torque control of an induction machine. In order to perform the optimal design, the objective function, which represents the design expectation, was developed. The objectives that were supposed to be fulfilled in this research were stated as sub objective functions including:
    i. Minimizing the deviation of the motor speed from the set value
    ii. Minimizing the torque ripple to have a smooth rotation of the shaft and reduce the mechanical stresses
    iii. Improve the quality of the dc link voltage while considering the size of filter elements

    PSCAD/EMTDC optimization tool (that uses simplex method) along with the multi-run feature was employed to find the optimum set of system parameters that result in the minimum value of objective function.
4. The value of the objective functions after and before the optimization in Table 4-2 demonstrate the improvement of the indirect vector controlled drive system performance during the transient and steady state operations. The speed error is reduced by nearly one-eleventh and the torque ripple is reduced approximately by half. At first the size of the filter elements was

chosen to be small, but the optimization showed that by increasing the Filter size within the acceptable range, the improvement in the dc voltage quality is considerable and this leads to reduce the torque ripple significantly.

5. Likewise, the improvement in constant switching DTC drive system performance can be observed by considering the value of objective functions before and after the optimization presented in Table 5-3.
6. Although the simulation base optimal design is a design method with minimum human interaction, it is a repetitive process of long time simulation runs that should be carrying with a small simulation time step. Moreover, the design expert should have several trial and error based simulation runs to obtain the initial set of parameters as well as the weight for sub objective functions which is also time consuming. In this research, it has been observed that the optimum point of minimum value of objective function in indirect vector control is found after 643 simulation runs taking 49200.90 seconds, and in case of direct torque control after 553 simulation run within 30648.00 seconds.
7. To overcome the challenge stated in part 6, reduced intensity computer models, including average value and mathematical models of power electronic inverters has been introduced as the solutions. The benefits of each model are explained as follows.
    i. In system-level study, the average value model can be used when the exact behaviour of the power switching devices is not a concern. Since the dynamic average value of the currents and voltages are

used instead of their instantaneous values in this method, higher order harmonics are eliminated and the time step can be chosen significantly less than the detailed model simulation case. Table 6-1 and Table 6-2 compare the average and detailed model simulation time for vector control and direct torque control respectively. It can be observed that using average model can reduce the simulation time by approximately one tenth.

ii. The mathematical model is based on the relationship between the input and output quantities of the power electronic inverter. In this case, to have accurate results the simulation time step cannot be less than the detailed model simulation case, since the output voltage is a function of the switching actions. Therefore it is more time consuming than the average model but provides the same results as the detailed model. Table 6-3 and Table 6-4 shows that the simulation time is reduced by approximately one third using mathematical model for vector control and direct torque control respectively.

7.2 Recommendations for Future work

Two related areas that can be considered as the possible expansion of this research is:

1. In order to optimize the performance of these systems, simplex method has been used in this research. This method and other conventional nonlinear optimization

algorithms offered by EMTDC provide a locally minimum of the objective function as the optimal solution. However it is preferable to detect and have access to all local minimum values of the objective function and subsequently the global minimum solution. The reason is that although the global optimum provides a superior performance of the system, for practical implementation of such systems, an optimal solution with less sensitivity to different operating conditions is desirable whether it is a local or global minimum.

There has been proposed algorithm [22] that can be used for this purpose. The problem is that in case of advanced drive systems that there are so many unknown parameters, due to limitation of maximum simulation run using multiple-run feature in PSCAD/EMTDC, it is not feasible to employing this algorithm for obtaining all the local and global minimum solutions.

2. Another potential solution that can be considered to reduce the computational intensity of simulation-based optimal design of drive systems is to develop accelerated optimization techniques. A low-intensity optimization algorithm will require a smaller number of computer simulations before it arrives at an optimal solution. A number of alternatives exist to create low-intensity algorithms including hybridization, where a low resolution algorithm is used to start the search followed by a high resolution algorithm to steer the final stages of the search.

References

[1] P. C. Sen, *Principles of Electric Machines and Power electronics*, 2nd edition, Wiley, 1996.

[2] B. K. Bose, *Modern Power Electronics and AC Drives*, Englewood Cliffs, NJ: Prentice-Hall, 2001.

[3] M. P. Kazmierkowski, R. Krishnan, and F. Blaabjerg, Eds., *Control in Power Electronics*. San Diego, CA: Academic, 2002.

[4] E. F Fuchs, M.A.S Masoum, *Power quality in Power system and Electrical Machines*, San Diego, CA: Academic Press, 2008.

[5] R. Krishnan, *Electric Motor Drives: Modeling, Analysis, and control*, Upper Saddle River, NJ: Prentice-Hall Inc., 2011.

[6] W. Leonard , *Control of Electric Drives*, 3rd Edition, Springer, 2001.

[7] I. ludtke, M. G. Jayne, "A comprehensive study of high performance speed control strategies for voltage sourced PWM inverter fed induction machine drives," *seventh international conference on electrical machines and drives*, 11-13 September 1995, University of Durham, UK.

[8] P. Vas, *Sensorless vector and direct torque control*, Oxford University Press, 1998.

[9] K. Ohnishi, H. Suzuki, K. Miyachi, M. Terashima, "Decoupling Control of Secondary Flux and Secondary Current in Induction Motor Drive with Controlled Voltage Source

and Its Comparison with Volts/Hertz Control," *IEEE Trans. Industry Applications,* vol. IA-21, no.1, pp.241-247, Jan. 1985.

[10] M. Heidari, "Decision Support Algorithms for Power System and Power Electronic Design," Ph.D. Dissertation, University of Manitoba, Winnipeg, Canada, 2010.

[11] S. Filizadeh, "Optimization-Enabled Electromagnetic Transient Simulation," Ph.D. Dissertation, University of Manitoba, Winnipeg, Canada, 2004.

[12] S. Filizadeh, A. M. Gole, "Optimal design of power electronic systems using electromagnetic transient simulation," in *Canadian Conference on Electrical and Computer Engineering,* 2005, pp. 450-453.

[13] A. M. Gole, S. Filizadeh, R. W. Menzies and P. L. Wilson, "Optimization-enabled electromagnetic transient simulation," *IEEE Trans. Power Delivery,* vol. 20, pp. 512-518, Jan 2005.

[14] M. Heidari, S. Filizadeh and A. M. Gole, "Support Tools for Simulation-Based Optimal Design of Power Networks with Embedded Power Electronics," *IEEE Trans. Power Delivery,* vol. 23, pp. 1561-1570, 2008.

[15] A. M. Gole, S. Filizadeh, R. W. Menzies and P. L. Wilson, "Optimization-enabled electromagnetic transient simulation," *IEEE Trans. Power Delivery,* vol. 20, pp. 512-518, 2005.

[16] S. Filizadeh, A. M. Gole, D. A. Woodford and G. D. Irwin, "An Optimization-Enabled Electromagnetic Transient Simulation-Based Methodology for HVDC Controller Design," *IEEE Trans. Power Delivery,* vol. 22, pp. 2559-2566, 2007.

[17] G. R. Slemon "Modeling of induction machines for electric drives," *IEEE Trans. Industry Applications,* vol.25, p.1126, 1989.

[18] P. C. Krause, O. Wasynczuk and S. D. Sudhoff, *Analysis of Electric Machinery and Drive Systems,* Wiley Inter-science, 2002.

[19] R. H. Park, "Two-reaction theory of synchronous machines generalized method of analysis-part I," *AIEE Tran.*, vol.48, no.3, pp.716-727, July 1929.

[20] J. G. Kassakian, M. F. Schlecht, G. C. Verghese, *Principles of Power Electronics*, Addison-Wesley, 1991.

[21] N. Mohan, T.M. Undeland, W.P. Robbins, *Power Electronics: Converters, Applications and Control*, Wiley, 2003.

[22] F. Yahyaie, "Simulation-Based Design of Multi-Model Systems," M.Sc. Dissertation, University of Manitoba, Winnipeg, Canada, 2010.

[23] J. Holtz, "Pulse width modulation – a survey," *IEEE Trans. Ind. Electron.*, vol.39, no. 5, pp. 410-420, Oct. 1992.

[24] A. Mehrizi-Sani, S. Filizadeh, "Digital implementation and transient simulation of space-vector modulated converters," *Power Engineering Society General Meeting, 2006. IEEE* , vol., no., pp.7 pp., 0-0 0.

[25] J. Holtz, "Pulsewidth modulation for electronic power conversion," *Proceedings of the IEEE*, vol. 82, no. 8, pp. 1194-1214, Aug. 1994.

[26] A. Mehrizi-Sani, "Advanced Modulation Techniques for Power Converters," M. Sc. Dissertation, University of Manitoba, Winnipeg, Canada, 2007.

[27] F. Boldea, S. A. Nasar, *Vector control of ac drives*, CRC Press Inc., Boca Raton, FL, 1992.

[28] Y. S. Lai, "Modeling and vector control of induction machines-a new unified approach," *Power Engineering Society 1999 Winter Meeting, IEEE*, vol.1, no., pp.47-52 vol.1, 31 Jan-4 Feb 1999.

[29] A. M. Trzynadlowski, *The Field Orientation Principle in Control of Induction Motors*, Kluwer Academic Publishers, Hingham, MA, 1994.

[30] N. P. Quang and J. Dittrich, *Vector Control of Three-Phase AC Machines: System Development in the Practice,* Springer, 2008.

[31] R. D. Lorenz, "Tuning of Field-Oriented Induction Motor Controllers for High-Performance Applications," *IEEE Tran. Industry Applications*, vol.IA-22, no.2, pp.293-297, March 1986.

[32] R. Krishnan, A.S. Bharadwaj, "A review of parameter sensitivity and adaptation in indirect vector controlled induction motor drive systems," *IEEE Trans. Power Electronics*, vol.6, no.4, pp.695-703, Oct 1991.

[33] R. Krishnan, F.C. Doran, "Study of Parameter Sensitivity in High-Performance Inverter-Fed Induction Motor Drive Systems," *IEEE Trans. Industry Applications,* vol. IA-23, no.4, pp.623-635, July 1987.

[34] P. Tiitinen, M. Surandra, "The next generation motor control method, DTC direct torque control," in *Proc. 1996 Power Electronics, Drives and Energy Systems for Industrial Growth, 1996.,* vol.1, no., pp.37-43 vol.1, 8-11 Jan 1996.

[35] M. Depenbrock, "Direct self-control (DSC) of inverter-fed induction machine," *IEEE Trans. Power Electronics,* vol.3, no.4, pp.420-429, Oct 1988.

[36] I. Takahashi, Y. Ohmori, "High-performance direct torque control of an induction motor," *IEEE Trans. Industry Applications,* vol.25, no.2, pp.257-264, Mar/Apr 1989.

[37] "Direct torque control—The world's most advanced AC drive technology," ABB Finland, Helsinki, Tech. Guide 1, 1996.

[38] M. P. Kazmierkowski, A. B. Kasprowicz, "Improved direct torque and flux vector control of PWM inverter-fed induction motor drives," *IEEE Trans. Industrial Electronics,* vol.42, no.4, pp.344-350, Aug 1995.

[39] M. Bertoluzzo, G. Buja, R. Menis, "Analytical formulation of the direct control of induction motor drives," in *Proc. 1999 Industrial Electronics, IEEE International Symposium*, vol.1, no., pp.PS14-PS20 vol.1, 1999.

[40] J. Maes, J. A. Melkebeek, "Speed-sensorless direct torque control of induction motors using an adaptive flux observer," *IEEE Trans. Industry Applications,* vol.36, no.3, pp.778-785, May/Jun 2000.

[41] M. S. Merzoug, F. Naceri "comparison of field-oriented control and Direct Torque Control for permanent magnet synchronous motor (PMSM), " *World Academy of science, Engineering and Technology 45*,pp.299-304, 2008.

[42] G. S. Buja, M. P. Kazmierkowski, "Direct torque control of PWM inverter-fed AC motors - a survey," *IEEE Trans. Industrial Electronics,* vol.51, no.4, pp. 744- 757, Aug. 2004.

[43] J. Hu, B. Wu , "New integration algorithms for estimating motor flux over a wide speed range," *IEEE Trans. Power Electronics,* vol.13, no.5, pp.969-977, Sep 1998.

[44] M. H. Shin; D.S. Hyun; S.B. Cho; S.Y. Choe, "An improved stator flux estimation for speed sensorless stator flux orientation control of induction motors," *IEEE Trans. Power Electronics,* vol.15, no.2, pp.312-318, Mar 2000.

[45] N. R. N. Idris, A. H. M. Yatim, "An improved stator flux estimation in steady-state operation for direct torque control of induction machines," *Industry Applications, IEEE Transactions on*, vol.38, no.1, pp.110-116, Jan/Feb 2002.

[46] T. G. Habetler, F. Profumo, M. Pastorelli, L.M. Tolbert, "Direct torque control of induction machines using space vector modulation," *IEEE Trans. Industry Applications,* vol.28, no.5, pp.1045-1053, Sep/Oct 1992.

[47] H. R. Keyhani, M. R. Zolghadri, A. Homaifar, "An extended and improved discrete space vector modulation direct torque control for induction motors," *Power Electronics Specialists Conf., 2004. PESC 04. 2004 IEEE 35th Annual* , vol.5, no., pp. 3414- 3420 Vol.5, 20-25 June 2004.

[48] F. M. Abdel-kader, A. El-Saadawi, A. E. Kalas, O. M. El-baksawi, "Study in direct torque control of induction motor by using space vector modulation," *Power System Conf., 2008. MEPCON 2008. 12th International Middle-East* , vol., no., pp.224-229, 12-15 March 2008.

[49] Y. S. Lai; J. H. Chen; , "A new approach to direct torque control of induction motor drives for constant inverter switching frequency and torque ripple reduction," *IEEE Tran. Energy Conversion,* vol.16, no.3, pp.220-227, Sep 2001.

[50] Y. Xue, X. Xu, T. G. Habetler, D.M. Divan, "A low cost stator flux oriented voltage source variable speed drive," in *Proc. 1990 IEEE Industry Applications Society Annual Meeting Conf.*, vol., no., pp.410-415 vol.1, 7-12 Oct 1990.

[51] S. Chiniforoosh, J. Jatskevich, A. Yazdani, V. Sood, V. Dinavahi, J.A. Martinez, A. Ramirez, "Definitions and Applications of Dynamic Average Models for Analysis of Power Systems," *IEEE Trans. Power Delivery,* vol.25, no.4, pp.2655-2669, Oct. 2010.

[52] A. Yazdani and R. Iravani "A generalized state-space averaged model of the three-level NPC converter for systematic DC-voltage-balancer and current-controller design," *IEEE Trans. Power Del.*, vol. 20, pp.1105 2005.

[53] "EMTDC manual," Winnipeg: Manitoba HVDC Research Center, 2003.

[54] H. W. Dommel "*EMTP Theory Book*," 1992 :MicroTran Power System Analysis Corp.